Correlations between bulk parameters in relativistic and nonrelativistic hadronic mean-field models

B. M. Santos,[1] M. Dutra,[2] O. Lourenço,[3] and A. Delfino[1]

[1]*Instituto de Física, Universidade Federal Fluminense, 24210-150 Niterói, Rio de Janeiro, Brazil*

[2]*Departamento de Ciências da Natureza, IHS, Universidade Federal Fluminense, 28895-532 Rio das Ostras, Rio de Janeiro, Brazil*

[3]*Departamento de Ciências da Natureza, Matemática e Educação, CCA, Universidade Federal de São Carlos, 13600-970 Araras, São Paulo, Brazil*

(Received 2 March 2015; revised manuscript received 31 May 2015; published 20 July 2015)

In this work, we study the arising of correlations among some isoscalar (K_o, Q_o, and I_o) and isovector (J, L_o, $K^o_{\rm sym}$, $Q^o_{\rm sym}$, and $I^o_{\rm sym}$) bulk parameters in nonrelativistic and relativistic hadronic mean-field models. For the former, we investigate correlations in Skyrme and Gogny parametrizations, as well as in the nonrelativistic (NR) limit of relativistic point-coupling models. We provide analytical correlations among bulk parameters for the NR limit, discussing the conditions in which they are linear ones. Based on a recent study [Santos *et al.*, Phys. Rev. C **90**, 035203 (2014)], we also show that some correlations presented in the NR limit are reproduced for relativistic models presenting cubic and quartic self-interactions in the scalar field σ, mostly studied in this work in the context of the relativistic framework. We also discuss how the crossing points, observed in the density dependence of some bulk parameters, can be seen as a signature of linear correlations between the specific bulk quantity presenting the crossing and its immediately next order parameter.

DOI: 10.1103/PhysRevC.92.015210 PACS number(s): 21.65.Mn, 13.75.Cs, 21.30.Fe, 21.60.−n

I. INTRODUCTION

In a general way, there are at least two different and competitive approaches in the treatment of nuclear matter. One of them is based on nucleon-nucleon interactions, from which many-nucleon microscopic relativistic/nonrelativistic Brueckner-Hartree-Fock (BHF) [1] calculations are performed to obtain information regarding the entire nuclear system. These calculations depend on the chosen nucleon-nucleon potential, classified as phenomenological (Reid, Urbana, and Argonne interactions, for instance) or theoretical one-boson exchange ones (Paris, Bonn, and Nijmegen interactions, for instance). For a short review, see Ref. [2]. Such nucleon-nucleon interactions reproduce experimental data on phase-shifts and deuteron properties and are implemented in complicated many-nucleon BHF codes to obtain nuclear matter properties. Alternatively, a second (macroscopic) approach does not use the nucleon-nucleon interaction itself. This is the case of nonrelativistic mean-field models like Skyrme [3] and Gogny [4] ones. In the relativistic framework, however, the most used models are the relativistic mean-field (RMF) Walecka model [5] and its improved versions [6].

In both approaches, many of the models and approximations used are intrinsically related to the fact that an analytical expression for the nucleon-nucleon potential is unknown. Therefore, in a theoretical point of view, correlations between two or more observables acquire enormous importance owing to the fact that they reduce the set of independent relevant quantities to be used in the construction of nuclear models, avoiding redundant free-parameter fittings. In an experimental point of view, however, a correlation between two observables $\mathcal{A}$ and $\mathcal{B}$, for instance, allows the complete knowledge of $\mathcal{B}$ if $\mathcal{A}$ is experimentally well constrained.

In the few-body nuclear physics, for example, the Tjon line [7] establishes a correlation between the binding energies of ^{4}He and triton, B_α and B_t, respectively. The parametrization of the numerical results for several two-nucleon potentials [8] concludes that such a correlation reads roughly $B_\alpha = 4.72(B_t - 2.48)$, in MeV units. It means that if B_t is calculated by using a two nucleon-nucleon potential, the value of B_α is predicted, even before any four-nucleon calculation.

Concerning correlations among bulk parameters, there are still a few of them well established in the literature. One of them, usually known as the Coester line [9], correlates the saturation density ρ_o and the nuclear matter binding energy B_o. It was analyzed in Ref. [9] in a two-nucleon model interaction by varying its tensor force contribution while keeping the deuteron binding energy fixed. They showed that the function $B_o \times \rho_o$ roughly follows a line, in fact a band, also observing its similarity with the curve constructed from B_o and ρ_o obtained from distinct two-nucleon potentials. Even modern calculations using BHF, and including single-particle contribution in the continuum, change the results but preserve the Coester line. Another correlation was studied in Ref. [10] and involves the relationship between finite nuclei spin-orbit splittings and the ratio $m^* = M^*_o/M$ for a class of finite-range (FR) RMF models, M^*_o being the nucleon Dirac effective mass at $\rho = \rho_o$ and M the nucleon rest mass. The authors showed that such splittings are experimentally well reproduced if the range for m^* is constrained to the following inequality:

$$0.58 \leqslant m^* \leqslant 0.64. \tag{1}$$

We refer to the above relation extracted from Ref. [10] as the FRS constraint. It is important because it relates bulk infinite nuclear matter calculation with the closed-shell finite nuclei energy spectrum. Still regarding relationships among quantities of finite nuclei and infinite nuclear matter, we also point out the correlation between the neutron skin thickness in ^{208}Pb, and the liquid-to-solid transition density in neutron-rich matter, investigated in Ref. [11] with RMF models.

In a recent paper [12], we provided analytical expressions linearly correlating the symmetry energy (J), its slope (L_o),

and curvature ($K^o_{\rm sym}$) at the saturation density in the framework of the nonrelativistic (NR) limit of nonlinear point-coupling (NLPC) versions of the Boguta-Bodmer models [13] (FR-RMF models presenting cubic and quartic self-interactions in the scalar field σ). From such analytical correlations, we were able to predict ranges for L_o that Boguta-Bodmer models must present to furnish good values for finite nuclei spin-orbit splittings. In this paper, we further investigate the arising of correlations among bulk parameters of infinite nuclear matter at zero temperature in nonrelativistic and relativistic hadronic mean-field models. For the former, we choose some Skyrme and Gogny parametrizations as well as the NR limit of NLPC models. For the latter, we choose FR-RMF models, especially the Boguta-Bodmer ones, and show the conditions to be satisfied for their bulk parameters present correlations. In particular, we show, in a general way, how linear correlations are connected with crossing points in the density dependence of bulk parameters. For this purpose, we generalize the procedure used in Ref. [14], where the authors associated the crossing point in the incompressibility function for different nonrelativistic Skyrme models, but not for FR-RMF ones, with the linear correlation between K_o and Q_o (incompressibility and skewness coefficient at ρ_o, respectively). We show here that there are other crossing densities different from $\rho_c \simeq 0.7\rho_o$—the value found in Refs. [14,15]—for different bulk parameters in nonrelativistic models, as well as in relativistic ones. In the following, we see that such crossing densities may be seen as signatures of linear correlations between higher-order derivatives of the specific bulk parameter presenting the crossing.

The paper is organized as follows. In Sec. II we show how linear correlations are connected with crossing densities in bulk parameters of infinite nuclear matter. In Sec. III, we use some results of our previous study of the NR limit [12] to apply the calculations of the previous section. In Sec. IV, we use the predictions of the NR limit to study the conditions that establish linear correlations in FR-RMF models. In Sec. V, we study relativistic and nonrelativistic models presenting two isovector coupling constants in the context of the correlation between the symmetry energy and its slope. Finally, we present our main conclusions in Sec. VI.

II. CONNECTION BETWEEN LINEAR CORRELATIONS AND CROSSING DENSITIES

In the literature, it is verified that crossing points can occur in the density dependence of the symmetry energy [16], in a pure neutron matter equation of state [17], and in a pairing gap of nuclear matter [18], for instance. Recently, in Refs. [14,15], the authors found a specific crossing point in the incompressibility of nuclear matter for different nonrelativistic Skyrme models, which is not confirmed in FR-RMF ones. They showed that this crossing density ($\rho_c \simeq 0.7\rho_o \simeq 0.11$ fm^{-3}), when used in the calculation of the derivative of the incompressibility, makes this quantity better correlated to the centroid energy of the isoscalar giant monopole resonance than K_o. The authors also pointed out that this crossing density ρ_c is closer to the average density in the ^{208}Pb nucleus, $\langle\rho\rangle = 0.12$ fm^{-3}, than the saturation density itself, $\rho_o \simeq 0.16$ fm^{-3}, with $\langle\rho\rangle$ also obtained by using the Skyrme model. The question we pose here is what properly means, or indicates, such crossing points. In the following, we try to answer this question.

Actually, crossing points in different bulk parameters of infinity nuclear matter can be viewed as a signature of linear correlations between higher-order derivatives of that particular bulk parameter presenting the crossing in its density dependence. To make it clear, we proceed to generalize the calculation performed in Ref. [14], where the authors associated a crossing in the $K(\rho)$ function with the linear correlation between K_o and Q_o for some Skyrme parametrizations. First, let us define a function of the density, $\mathcal{F}(\rho)$, expanded in terms of the dimensionless variable $x = \frac{\rho-\rho_o}{3\rho_o}$ and around the saturation density as

$$\mathcal{F}(\rho) = \mathcal{F}(\rho_o) + \mathcal{F}'(\rho_o)x + \frac{\mathcal{F}''(\rho_o)}{2!}x^2 + \frac{\mathcal{F}'''(\rho_o)}{3!}x^3 + \cdots, \tag{2}$$

with the derivatives of $\mathcal{F}(\rho)$ given by

$$\mathcal{F}^{(m)}(\rho) = (3\rho)^m \frac{\partial}{\partial\rho}\left[\frac{\mathcal{F}^{(m-1)}(\rho)}{(3\rho)^{m-1}}\right] \tag{3}$$

for $m = 1,2,3,\ldots$.

For the values $m = 1,2,3$, for instance, and by noting that $\frac{\rho}{\rho_o} = 3x + 1$ and $\frac{\partial}{\partial\rho} = \frac{\partial x}{\partial\rho}\frac{\partial}{\partial x} = \frac{1}{3\rho_o}\frac{\partial}{\partial x}$, we see that Eq. (3) leads to

$$\mathcal{F}'(\rho) = 3\rho\frac{\partial\mathcal{F}}{\partial\rho} = \frac{3\rho}{3\rho_o}\frac{\partial\mathcal{F}}{\partial x} = (3x+1)\frac{\partial\mathcal{F}}{\partial x}, \tag{4}$$

$$\begin{aligned}\mathcal{F}''(\rho) &= (3\rho)^2\frac{\partial}{\partial\rho}\left[\frac{\mathcal{F}'(\rho)}{3\rho}\right] = (3\rho)^2\frac{\partial}{\partial\rho}\left[\frac{\partial\mathcal{F}}{\partial\rho}\right] \\ &= \frac{(3\rho)^2}{(3\rho_o)^2}\frac{\partial^2\mathcal{F}}{\partial x^2} = (3x+1)^2\frac{\partial^2\mathcal{F}}{\partial x^2},\end{aligned} \tag{5}$$

and

$$\begin{aligned}\mathcal{F}'''(\rho) &= (3\rho)^3\frac{\partial}{\partial\rho}\left[\frac{\mathcal{F}''(\rho)}{(3\rho)^2}\right] = (3\rho)^3\frac{\partial}{\partial\rho}\left[\frac{\partial^2\mathcal{F}}{\partial\rho^2}\right] \\ &= \frac{(3\rho)^3}{(3\rho_o)^3}\frac{\partial^3\mathcal{F}}{\partial x^3} = (3x+1)^3\frac{\partial^3\mathcal{F}}{\partial x^3}.\end{aligned} \tag{6}$$

The pattern verified in Eqs. (2)–(6) allows us to write $\mathcal{F}(\rho)$ and its derivatives in a compact form as

$$\begin{aligned}\mathcal{F}^{(m)}(\rho) = (3x+1)^m\Bigg\{&\mathcal{F}^{(m)}(\rho_o) + \mathcal{F}^{(m+1)}(\rho_o)x \\ &+ \frac{\mathcal{F}^{(m+2)}(\rho_o)}{2!}x^2 + \frac{\mathcal{F}^{(m+3)}(\rho_o)}{3!}x^3 + \cdots\Bigg\},\end{aligned} \tag{7}$$

for $m = 0,1,2,3,\ldots$, and with $\mathcal{F}^{(m)}(\rho_o)$, $\mathcal{F}^{(m+1)}(\rho_o)$, $\mathcal{F}^{(m+2)}(\rho_o)$, $\ldots$, being the bulk parameters evaluated at the saturation density.

To make our analysis simpler, we consider that $\mathcal{F}^{(m)}/(3x+1)^m$ is well described by its expansion until order x^3. Now let us assume that the bulk parameters of the higher-order derivatives of $\mathcal{F}^{(m)}$, namely, $\mathcal{F}^{(m+1)}(\rho_o)$, $\mathcal{F}^{(m+2)}(\rho_o)$, and $\mathcal{F}^{(m+3)}(\rho_o)$, are correlated with $\mathcal{F}^{(m)}(\rho_o)$, more specifically in a

linear way, as

$$\mathcal{F}^{(m+1)}(\rho_o) = b_1 + a_1\mathcal{F}^{(m)}(\rho_o), \tag{8}$$

$$\mathcal{F}^{(m+2)}(\rho_o) = b_2 + a_2\mathcal{F}^{(m)}(\rho_o), \tag{9}$$

$$\mathcal{F}^{(m+3)}(\rho_o) = b_3 + a_3\mathcal{F}^{(m)}(\rho_o), \tag{10}$$

with a_i and b_i independent of any other parameters of the model. If such linear correlations hold, then Eq. (7) can be rewritten as

$$\mathcal{F}^{(m)}(\rho) \simeq (3x+1)^m \left\{ f(x)\mathcal{F}^{(m)}(\rho_o) + b_1 x + \frac{b_2}{2!}x^2 + \frac{b_3}{3!}x^3 \right\}, \tag{11}$$

where

$$f(x) = 1 + a_1 x + \frac{a_2}{2!}x^2 + \frac{a_3}{3!}x^3. \tag{12}$$

For a specific value (or values) of the density, named as ρ_c, that makes $f(x_c) = 0$, with $x_c = \frac{\rho_c - \rho_o}{3\rho_o}$, $\mathcal{F}^{(m)}(\rho_c)$ will be exactly the same for any hadronic model, according to Eq. (11) because the b_i parameters are model independent. Therefore, the functions $\mathcal{F}^{(m)}(\rho)$ of any model will cross each other exactly at $\rho = \rho_c$. This is the crossing point presented in the $\mathcal{F}^{(m)}(\rho)$ function. Thus, one can see this crossing as a signature of the linear correlations given by Eqs. (8)–(10). Naturally, such a signature only holds if we can express the function $\mathcal{F}^{(m)}(\rho)$ in terms of the expansion presented in Eq. (7).

In the case where $\mathcal{F}^{(m)}/(3x+1)^m$ is expanded until order x^3, Eq. (12) generates a cubic equation, when one imposes $f(x_c) = 0$, to localize the values of ρ_c. In the general case, in which it is necessary to expand $\mathcal{F}^{(m)}/(3x+1)^m$ until order x^N, then

$$f(x_c) = 1 + \sum_{i=1}^{N} \frac{a_i x_c^i}{i!} = 0 \tag{13}$$

produces an equation of order N to be solved to determine the possible values of x_c, and, consequently, the crossing densities ρ_c of the function $\mathcal{F}^{(m)}(\rho)$.

The determination of linear correlations from the searching of crossing points is suitable, for instance, for the isovector bulk properties of hadronic models, in which the quantities and their derivatives can be expanded around the saturation density exactly as in Eq. (7). The energy per particle of a system of proton fraction given by $y = \rho_p/\rho$ (ρ_p is the proton density) can be expanded in terms of the isospin asymmetry parameter $\beta = 1 - 2y$ as

$$E(\rho,\beta) = E(\rho) + \mathcal{S}(\rho)\beta^2 + \mathcal{S}_4(\rho)\beta^4 + \cdots, \tag{14}$$

where $E(\rho)$ is the energy per particle related to the symmetric nuclear matter ($\beta = 0$). The other two coefficients of the expansion are, respectively, the symmetry energy and the fourth-order symmetry energy, with the density dependence, associated with the isovector sector, expanded in terms of the density as

$$\mathcal{S}(\rho) = J + L_o x + \frac{K^o_{\rm sym}}{2!}x^2 + \frac{Q^o_{\rm sym}}{3!}x^3 + \cdots \tag{15}$$

and

$$\mathcal{S}_4(\rho) = J_4 + L^o_4 x + \frac{K^o_{\rm sym,4}}{2!}x^2 + \frac{Q^o_{\rm sym,4}}{3!}x^3 + \cdots. \tag{16}$$

The derivatives of $\mathcal{S}(\rho)$ are defined exactly as in Eq. (3); i.e., $L = 3\rho\frac{\partial\mathcal{S}}{\partial\rho}$, $K_{\rm sym} = (3\rho)^2\frac{\partial^2\mathcal{S}}{\partial\rho^2}$, $Q_{\rm sym} = (3\rho)^3\frac{\partial^2\mathcal{S}}{\partial\rho^3}$, and so on. The isovector bulk parameters, L_o, $K^o_{\rm sym}$, and $Q^o_{\rm sym}$, are the derivatives evaluated at $\rho = \rho_o$, and J is given by $J = \mathcal{S}(\rho_o)$. Analogous quantities are also defined from $\mathcal{S}_4(\rho)$. Based on this structure, the search of linear correlations from the location of crossing densities can be naturally performed. This will be done for nonrelativistic and relativistic models in the next two sections.

As a last remark, we mention here that the procedure described above was first used in Ref. [14] specifically to justify the crossing point in the $K(\rho) \times \rho$ curve, and not as a route to find linear correlations as we are doing in the present work. Moreover, we are also generalizing this method to any bulk parameter.

III. CORRELATIONS IN NONRELATIVISTIC MODELS

A. Theoretical framework of the NR limit

In the background of nonrelativistic mean-field models, we analyze some parametrizations of Skyrme and Gogny models and also those from the NR limit of NLPC versions of the Boguta-Bodmer model. It is important to mention that as the FR-RMF models, relativistic point-coupling ones also describe very well the infinite nuclear matter bulk parameters and finite nuclei properties [19–24]. In Ref. [24], for instance, the authors were able to obtain, by using a NLPC model, ground-state binding energies, spin-orbit splittings, and rms charge radii of a large set of closed-shell nuclei, as well as those of nuclei outside the valley of β stability, clearly showing the success of these kinds of models. Their nonrelativistic versions, besides following this same pattern, at least concerning the infinite nuclear matter that is the focus of our work, are also useful in the sense that they can be used to predict correlations also exhibited in FR-RMF models, as observed in our previous study [12].

The relativistic NLPC versions of the Boguta-Bodmer models are described by a Lagrangian density,

$$\begin{aligned}\mathcal{L}_{\rm NLPC} = {} & \bar\psi(i\gamma^\mu\partial_\mu - M)\psi - \frac{1}{2}G_{\rm V}^2(\bar\psi\gamma^\mu\psi)^2 \\ & + \frac{1}{2}G_{\rm S}^2(\bar\psi\psi)^2 + \frac{A}{3}(\bar\psi\psi)^3 + \frac{B}{4}(\bar\psi\psi)^4 \\ & - \frac{1}{2}G_{\rm TV}^2(\bar\psi\gamma^\mu\vec\tau\psi)^2,\end{aligned} \tag{17}$$

that mimics the two-, three-, and four-body pointlike interactions. In this equation, the last term is included to take into account the asymmetry of the system (different number of protons and neutrons). In the NR limit of the NLPC model, and by using the mean-field approximation, the energy density functional at zero temperature for asymmetric nuclear matter

is written as

$$\varepsilon^{(\mathrm{NR})}(\rho,y) = \left(G_{\mathrm{V}}^2 - G_{\mathrm{S}}^2\right)\rho^2 - A\rho^3 - B\rho^4 + G_{\mathrm{TV}}^2\rho^2(2y-1)^2 + \frac{3}{10M^*(\rho,y)}\lambda\rho^{\frac{5}{3}}, \quad (18)$$

where the effective mass is

$$M^*(\rho,y) = \frac{M^2}{\left(M + G_{\mathrm{S}}^2\rho + 2A\rho^2 + 3B\rho^3\right)H_{\frac{5}{3}}}, \quad (19)$$

with $H_{\frac{5}{3}} = 2^{\frac{2}{3}}[y^{\frac{5}{3}} + (1-y)^{\frac{5}{3}}]$ and $\lambda = (3\pi^2/2)^{\frac{2}{3}}$; see Ref. [12].

From the energy density in Eq. (18), it is possible to obtain pressure, incompressibility, and the symmetry energy of the model, because $P = \rho^2\frac{\partial(\mathcal{E}/\rho)}{\partial\rho}$, $K = 9\frac{\partial P}{\partial\rho}$, and $\mathcal{S} = \frac{1}{8}[\frac{\partial^2(\varepsilon/\rho)}{\partial y^2}]_{y=\frac{1}{2}}$. These expressions are, respectively, given by

$$P^{(\mathrm{NR})}(\rho,y) = \left(G_{\mathrm{V}}^2 - G_{\mathrm{S}}^2\right)\rho^2 - 2A\rho^3 - 3B\rho^4 + G_{\mathrm{TV}}^2\rho^2(2y-1)^2 + \frac{\lambda H_{5/3}}{5M^2} \times \left(M + \frac{5}{2}G_{\mathrm{S}}^2\rho + 8A\rho^2 + \frac{33}{2}B\rho^3\right)\rho^{\frac{5}{3}}, \quad (20)$$

$$K^{(\mathrm{NR})}(\rho,y) = 18\left(G_{\mathrm{V}}^2 - G_{\mathrm{S}}^2\right)\rho - 54A\rho^2 - 108B\rho^3 + 18G_{\mathrm{TV}}^2\rho(2y-1)^2 + \frac{3\lambda H_{5/3}}{M^2} \times \left(M + 4G_{\mathrm{S}}^2\rho + \frac{88}{5}A\rho^2 + \frac{231}{5}B\rho^3\right)\rho^{\frac{2}{3}}, \quad (21)$$

and

$$\mathcal{S}^{(\mathrm{NR})}(\rho) = G_{\mathrm{TV}}^2\rho + \frac{\lambda\rho^{\frac{2}{3}}}{6M^*(\rho,1/2)}. \quad (22)$$

The symmetry energy $\mathcal{S}^{(\mathrm{NR})}$ is used to obtain its slope, curvature, and skewness. The results are

$$L^{(\mathrm{NR})}(\rho) = \frac{\lambda\rho^{\frac{2}{3}}}{3M^2}\left(M + \frac{5}{2}G_{\mathrm{S}}^2\rho + 8A\rho^2 + \frac{33}{2}B\rho^3\right) + 3G_{\mathrm{TV}}^2\rho, \quad (23)$$

$$K_{\mathrm{sym}}^{(\mathrm{NR})}(\rho) = \frac{\lambda\rho^{\frac{2}{3}}}{3M^2}\left(-M + 5G_{\mathrm{S}}^2\rho + 40A\rho^2 + 132B\rho^3\right), \quad (24)$$

and

$$Q_{\mathrm{sym}}^{(\mathrm{NR})}(\rho) = \frac{4\lambda\rho^{\frac{2}{3}}}{3M^2}\left(M - \frac{5}{4}G_{\mathrm{S}}^2\rho + 20A\rho^2 + 165B\rho^3\right), \quad (25)$$

respectively.

The coupling constants of the model are G_{S}^2, G_{V}^2, A, B, and G_{TV}^2. The first four of them are adjusted to fix ρ_o, B_o, K_o, and M_o^*. This is done by solving a system of four equations, namely, $\varepsilon^{(\mathrm{NR})}(\rho_o,1/2)/\rho_o = -B_o$, $K^{(\mathrm{NR})}(\rho_o,1/2) = K_o$, $P^{(\mathrm{NR})}(\rho_o,1/2) = 0$ (nuclear matter saturation), and $M^*(\rho_o,1/2) = M_o^*$. The last coupling constant, G_{TV}^2, is obtained by imposing upon the model the requirement of presenting a particular value for $J = \mathcal{S}^{(\mathrm{NR})}(\rho_o)$. The explicit forms of the constants G_{S}^2, G_{V}^2, A, B, and G_{TV}^2 in terms of m^*, ρ_o, B_o, K_o, and J are given in the Appendix.

B. Results from the isovector sector

In Ref. [12], we rewrote the coupling constants of the model in terms of the bulk parameters m^*, ρ_o, B_o, and K_o (an analogous procedure is done in the context of the Skyrme models in Ref. [25]). This method allowed us to explicitly write the slope of the symmetry energy at the saturation density also as a function of m^*, ρ_o, B_o, and K_o and, thus, find the following correlation between J and L_o, namely,

$$L_o = 3J + b(m^*,\rho_o,B_o,K_o), \quad (26)$$

with

$$b(m^*,\rho_o,B_o,K_o) = \frac{1}{\left(3M^2 - 19E_{\mathrm{F}}^oM + 18E_{\mathrm{F}}^{o2}\right)}\left\{\frac{10E_{\mathrm{F}}^o}{9m^*}\left(3M^2 - 14ME_{\mathrm{F}}^o\right) - 5E_{\mathrm{F}}^o\left(M^2 - 5ME_{\mathrm{F}}^o\right) + 30B_oE_{\mathrm{F}}^{o2} - \frac{5K_o}{9}E_{\mathrm{F}}^oM\right\}, \quad (27)$$

where $E_{\mathrm{F}}^o = 3\lambda\rho_o^{\frac{2}{3}}/10M$.

The expression in Eq. (24) along with the correlation in Eq. (26) and the definitions of the coupling constants in terms of the bulk parameters are used to find

$$K_{\mathrm{sym}}^o = (L_o - 3J)p(\rho_o) + q(\rho_o,B_o,K_o), \quad (28)$$

where

$$p(\rho_o) = \frac{3\left(5M^2 - 18E_{\mathrm{F}}^oM\right)}{3M^2 - 14ME_{\mathrm{F}}^o} \quad (29)$$

and

$$q(\rho_o,B_o,K_o) = \frac{5M^2E_{\mathrm{F}}^o + 90B_oME_{\mathrm{F}}^o - \frac{70}{9}K_oE_{\mathrm{F}}^oM}{3M^2 - 14ME_{\mathrm{F}}^o}. \quad (30)$$

As pointed out in Ref. [12], if J and K_o are kept fixed in Eq. (28), K_{sym}^o will present a linear correlation with L_o, because the binding energy and the saturation density are well established closely around the values of $B_o = 16$ MeV and $\rho_o = 0.15\ \mathrm{fm}^{-3}$ and do not vary too much for each parametrization of any nuclear mean-field model. For this reason, we consider B_o and ρ_o as constants hereafter. The same conditions also occur with the skewness of $\mathcal{S}$ of the NR limit, owing to its analytical structure in Eq. (25). This quantity, obtained through $Q_{\mathrm{sym}}^o = Q_{\mathrm{sym}}^{(\mathrm{NR})}(\rho_o)$, can also be written in the form

$$Q_{\mathrm{sym}}^o = (L_o - 3J)u(\rho_o) + v(\rho_o,B_o,K_o), \quad (31)$$

with

$$u(\rho_o) = -\frac{5\left(3M^2 - 22E_{\mathrm{F}}^oM - 144E_{\mathrm{F}}^{o2}\right)}{3M^2 - 14ME_{\mathrm{F}}^o}, \quad (32)$$

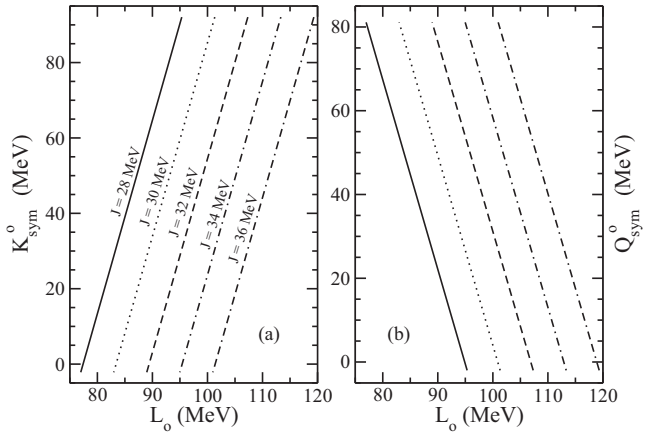

FIG. 1. (a) $K^o_{\rm sym}$ and (b) $Q^o_{\rm sym}$ as a function of L_o for the NR limit for different values of J. The effective mass varies in the range of $0.50 \leqslant m^* \leqslant 0.80$. For each panel, $\rho_o = 0.15$ fm^{-3}, $B_o = 16$ MeV, and $K_o = 270$ MeV.

and

$$v(\rho_o, B_o, K_o) = \frac{1}{3M^2 - 14ME^o_{\rm F}}\left\{5E^o_{\rm F}M\left(M + 52E^o_{\rm F}\right) - \frac{850}{9}K_oE^o_{\rm F}M + 150B_oE^o_{\rm F}\left(9M - 8E^o_{\rm F}\right)\right\}. \quad (33)$$

The linear dependence of $K^o_{\rm sym}$ and $Q^o_{\rm sym}$ as a function of L_o for fixed J and K_o is depicted in Fig. 1.

We remark to the reader that it was possible to investigate how $K^o_{\rm sym}$ and $Q^o_{\rm sym}$ depend on L_o by using parametrizations presenting J fixed and different values of the effective mass, specifically in the range of $0.50 \leqslant m^* \leqslant 0.80$. In this way, it was possible to keep J fixed and still be able to vary L_o from the variation of $b(m^*, \rho_o, B_o, K_o)$ in Eq. (26).

The increasing of $K^o_{\rm sym}$, and decreasing of $Q^o_{\rm sym}$ as a function of L_o, are also verified for Gogny interactions presented in Ref. [26]. In this work, the authors analyzed the isovector properties of this specific nonrelativistic model, providing analytical expressions for symmetric and asymmetric nuclear matter; see Fig. 2. Notice that although some parametrizations present a linear dependence, this behavior is not verified for all of them.

According to the discussion of Sec. II, the searching of such linear correlations could also have been done if we had looked for their possible signature, in this case in the density dependence of the symmetry energy slope. If the function $L^{(\rm NR)}(\rho)$ can be expanded and if its density dependence presents a crossing point, then one can ensure at least the linear behavior presented in Fig. 1(a). In fact, this crossing around $\rho^{\rm L}_c/\rho_0 = 0.47$ is verified in Fig. 3 in the NR limit for parametrizations in which the values of J and K_o are kept fixed.

It is worthwhile to note that the crossing density displayed in Fig. 3, namely, $\rho^{\rm L}_c/\rho_0 = 0.47$, is exactly the same for all curves. In this figure, we group three different sets of parametrizations, each one presenting three distinct values for the pair (J, K_o). The values were chosen inside the ranges of $25 \leqslant J \leqslant 35$ MeV, and $250 \leqslant K_o \leqslant 315$ MeV. One can

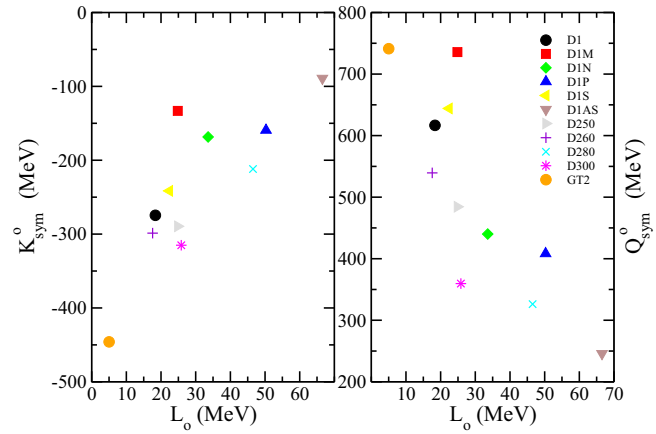

FIG. 2. (Color online) (a) $K^o_{\rm sym}$ and (b) $Q^o_{\rm sym}$ as a function of L_o for Gogny parametrizations studied in Ref. [26].

still notice that the quantity $L^{(\rm NR)}(\rho^{\rm L}_c)$ is different for each set. However, the values of $L^{(\rm NR)}(\rho^{\rm L}_c)$ of these parametrizations present an overlap of 48% with the constraint established in Ref. [27], namely, $L(\rho^{\rm L}_c) = 47.3 \pm 7.8$ MeV. We still point out that the range of $25 \leqslant J \leqslant 35$ MeV is shown to be totally compatible [6] with experimental values from analyses of different terrestrial nuclear experiments and astrophysical observations [28], and the range of $250 \leqslant K_o \leqslant 315$ MeV was based on the recent reanalysis of data on isoscalar giant monopole resonance energies [29].

If we consider the expansion of $L^{(\rm NR)}/(3x+1)$ until order x, namely, $L(\rho) \simeq (3x+1)(L_o + K^o_{\rm sym}x)$, it is possible to explain the crossing point in Fig. 3 if $K^o_{\rm sym}$ is linearly correlated with L_o, i.e., if we can write $K^o_{\rm sym} = b_1 + a_1L_o$, and if there exist a real root for the equation $f(x_c) = a_1x_c + 1 = 0$, because in this case one writes $L(\rho) = (3x+1)\{L_o(a_1x+1) + b_1x\}$. As we can see in Eq. (28) and in Fig. 1(a), the linear correlation between $K^o_{\rm sym}$ and L_o holds, in fact, for J and K_o fixed. However, if we solve the equation $f(x_c) = 0$ we find $\rho^{\rm L}_c/\rho_0 = 0.41$ [because $a_1 = p(\rho_o) = 5.13$ and $\rho^{\rm L}_c/\rho_0 = 3x^{\rm L}_c + 1$], not

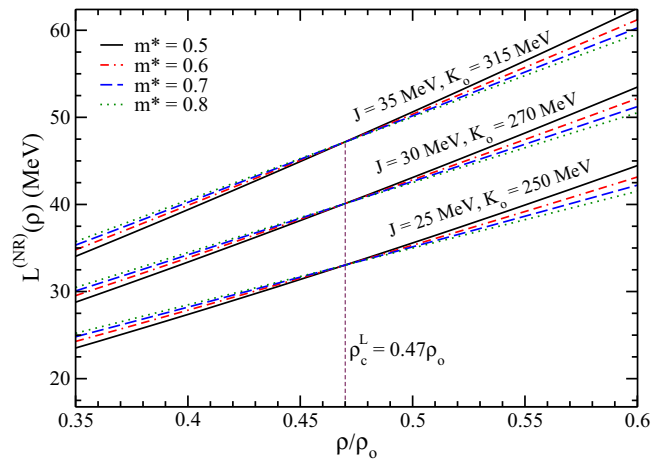

FIG. 3. (Color online) Symmetry energy slope as a function of ρ/ρ_o for the NR limit, Eq. (23). In this figure, $\rho_o = 0.15$ fm^{-3} and $B_o = 16$ MeV.

exactly the same crossing density presented in Fig. 3. This suggests that $f(x_c)$ should be modified to produce a more exact root, which means that $L^{(\mathrm{NR})}/(3x+1)$ actually needs to be expanded in higher orders in x, at least in the density region around the crossing density $\rho_c^{\mathrm{L}}/\rho_0 = 0.47$. If we now take the expansion of $L^{(\mathrm{NR})}/(3x+1)$ until order x^2, the crossing point will exist if K^o_{sym} and Q^o_{sym} are linearly correlated with L_o. The latter correlation is verified in Eq. (31) and Fig. 1(b), as we already discussed. For this case we will have

$$L(\rho) \simeq (3x+1)\left\{L_o + K^o_{\mathrm{sym}}x + \frac{Q^o_{\mathrm{sym}}}{2}x^2\right\} = (3x+1)\left\{L_o\left(\frac{a_2}{2}x^2 + a_1x + 1\right) + \left(\frac{b_2}{2}x + b_1\right)x\right\}, \tag{34}$$

with $b_1 = q - 3Jp$, $a_1 = p$, $b_2 = v - 3Ju$, and $a_2 = u$. The crossing is explained if $f(x_c^{\mathrm{L}}) = 1 + px_c^{\mathrm{L}} + \frac{u}{2}x_c^{\mathrm{L}2} = 0$, satisfied for

$$x_c^{\mathrm{L}} = \frac{1}{5\left(3M^2 - 22E^o_{\mathrm{F}}M - 144E^{o2}_{\mathrm{F}}\right)} \times \left\{15M^2 - 54E^o_{\mathrm{F}}M - \left(315M^4 - 2700E^o_{\mathrm{F}}M^3 + 1676E^{o2}_{\mathrm{F}}M^2 + 20160E^{o3}_{\mathrm{F}}M\right)^{\frac{1}{2}}\right\}, \tag{35}$$

which produces $\rho_c^{\mathrm{L}}/\rho_0 = 0.46$, a value much more close to the crossing density than $\rho_c^{\mathrm{L}}/\rho_0 = 0.41$, found previously.

Therefore, it becomes clear that a crossing point in a density dependence of a bulk parameters indicates a route for the searching of linear correlations in its higher-order derivatives. Nevertheless, we point out to the reader that a crossing point itself does not ensure linear correlations in all higher-order bulk parameters. For the previous analysis, for example, one cannot affirm that L_o will be correlated with $I^o_{\mathrm{sym}} = (3\rho_o)^4\left(\frac{\partial^4\mathcal{S}}{\partial\rho^4}\right)_{\rho=\rho_o}$ simply by the fact that the expansion of $L^{(\mathrm{NR})}/(3x+1)$ until order x^3 is better than those until order x^2. It is needed to check whether such linear correlation really holds. Actually, the crossing ensures at least the linear correlation between L_o and the immediately next order bulk parameter K^o_{sym}. As a matter of fact, we investigate if L_o correlates with I^o_{sym} by obtaining the expression of the fourth-order derivative of $\mathcal{S}^{(\mathrm{NR})}$, namely,

$$I^{(\mathrm{NR})}_{\mathrm{sym}}(\rho) = \frac{28\lambda\rho^{\frac{2}{3}}}{3M^2}\left(-M + \frac{5}{7}G_{\mathrm{S}}^2\rho - \frac{20}{7}A\rho^2 + \frac{330}{7}B\rho^3\right). \tag{36}$$

From Eq. (36), is possible to write $I^o_{\mathrm{sym}} = I^{(\mathrm{NR})}_{\mathrm{sym}}(\rho_o)$ in terms of L_o, J, ρ_o, B_o, and K_o as

$$I^o_{\mathrm{sym}} = (L_o - 3J)r(\rho_o) + s(\rho_o, B_o, K_o), \tag{37}$$

with

$$r(\rho_o) = \frac{20\left(3M^2 - 56ME^o_{\mathrm{F}} + 324E^{o2}_{\mathrm{F}}\right)}{3M^2 - 14ME^o_{\mathrm{F}}}, \tag{38}$$

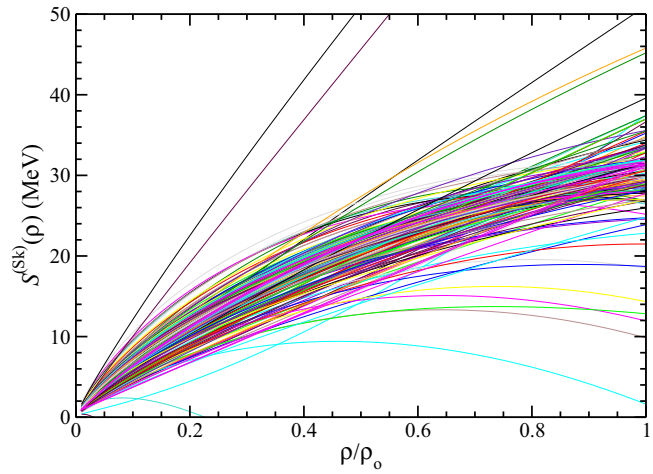

FIG. 4. (Color online) Symmetry energy as a function of ρ/ρ_o for the 240 Skyrme parametrizations of Ref. [3].

and

$$s(\rho_o, B_o, K_o) = \frac{5}{3M^2 - 14ME^o_{\mathrm{F}}}\left\{1080B_oE^o_{\mathrm{F}}\left(M - 2E^o_{\mathrm{F}}\right) - 12E^o_{\mathrm{F}}M\left(M - 18E^o_{\mathrm{F}}\right) - \frac{160}{3}K_oE^o_{\mathrm{F}}M\right\}. \tag{39}$$

Thus, it is verified that I^o_{sym} also linearly correlates with L_o, under the same conditions that makes L_o also correlated with K^o_{sym} and Q^o_{sym}, namely, fixed values for J and K_o. Furthermore, a new expansion of $L^{(\mathrm{NR})}/(3x+1)$ until order x^3 generates the cubic equation $f(x_c^{\mathrm{L}}) = 1 + px_c^{\mathrm{L}} + \frac{u}{2!}x_c^{\mathrm{L}2} + \frac{r}{3!}x_c^{\mathrm{L}3} = 0$, presenting a root corresponding to $\rho_c^{\mathrm{L}}/\rho_0 = 0.47$ [because $r(0.15) = 14.17$], the exact value for the crossing density.

Following these same ideas, we search for signatures of linear correlations in the Skyrme model. At this point, we remind the reader there is no unique crossing point at the density dependence of the symmetry energy and its slope for the Skyrme model, as we can see in Figs. 4 and 5, respectively, where we display the 240 parametrizations of Ref. [3].

This lack of a unique crossing in the density dependence of $\mathcal{S}(\rho)$ and $L(\rho)$ functions can also be seen in Fig. 2 (left) of Ref. [30], where the authors studied 21 Skyrme parametrizations.

Specifically for the density dependence of the symmetry energy slope, we found a crossing density for the SV [31], SkO [32], SkO′ [32], SkT3 [33], SkRA [34], and Ska35s15 [3] parametrizations at $\rho_c^{\mathrm{L}}/\rho_0 = 0.38$. It is displayed in Fig. 6.

According to the discussed so far, these Skyrme parametrizations will present linear correlation at least regarding K^o_{sym} and L_o. This is confirmed in Fig. 7(a). Moreover, in Figs. 7(b) and 7(c) it is also checked the linear correlations of L_o with Q^o_{sym} and I^o_{sym}, respectively, like in the case of the NR limit. For the sake of completeness, we have checked

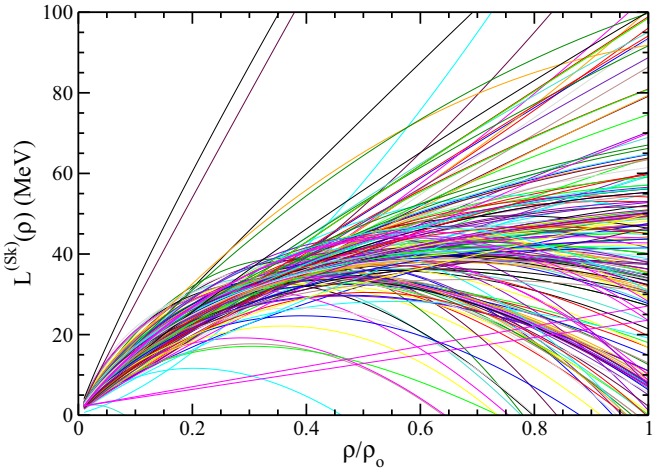

FIG. 5. (Color online) Symmetry energy slope as a function of ρ/ρ_o for the 240 Skyrme parametrizations of Ref. [3].

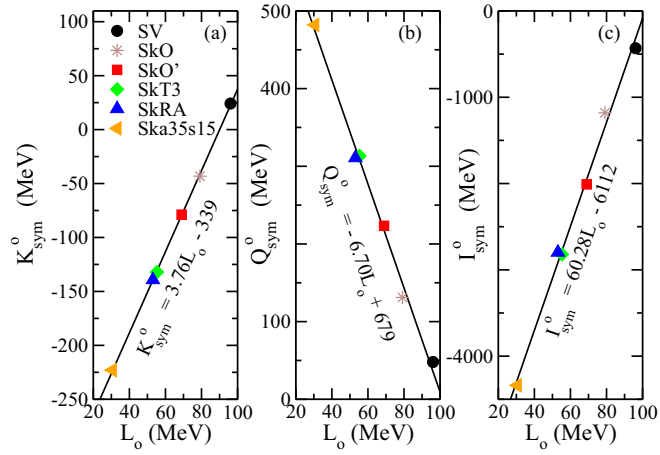

FIG. 7. (Color online) (a) $K^o_{\rm sym}$, (b) $Q^o_{\rm sym}$, and (c) $I^o_{\rm sym}$ as a function of L_o for the Skyrme parametrizations of Fig. 6. The linear fits are indicated in each panel.

that the expansion of $L(\rho)/(3x+1)$ that approaches to the exact function around $\rho/\rho_o = 0.38$ is taken until order x^3 for these Skyrme parametrizations. Therefore, the angular coefficients found in Fig. 7 are used to define the function $f(x_c^{\rm L})$ that needs to be null. This will provide the cubic equation $1 + 3.76x_c^{\rm L} - \frac{6.70}{2!}x_c^{\rm L\,2} + \frac{60.28}{3!}x_c^{\rm L\,3} = 0$, which has one of the roots given by $\rho_c^{\rm L}/\rho_0 = 0.38$, precisely the crossing density verified in Fig. 6.

Still at the framework of the Skyrme parametrizations, another crossing point is observed in the isovector sector, specifically in the density dependence of the symmetry energy itself. As pointed out in Fig. 8, such a crossing occurs at $\rho_c^{\rm S}/\rho_0 = 0.89$. We have noticed that for these parametrizations, J is linearly correlated with L_o, $K^o_{\rm sym}$, $Q^o_{\rm sym}$, and $I^o_{\rm sym}$, as one can see in Figs. 9 and 10. The angular coefficients of these lines are used to define the quartic equation to be solved to determine the value of the crossing density, namely, $1 + 28.8x_c^{\rm S} + \frac{108.6}{2!}x_c^{\rm S\,2} - \frac{188.3}{3!}x_c^{\rm S\,3} + \frac{1695}{4!}x_c^{\rm S\,4} = 0$. One root of this equation provides the value $\rho_c^{\rm S}/\rho_0 = 0.89$, observed in Fig. 8.

As a remark, it is worthwhile to note that a linear correlation itself between two bulk parameters is not a sufficient condition to guarantee a crossing point in the density dependence of the immediately preceding bulk parameter. As an example of this statement, we focus on the analytical structure of the NR limit to find other two specific linear correlations. From Eqs. (28) and (31) it is straightforward to obtain

$$Q^o_{\rm sym} = \frac{u}{p}K^o_{\rm sym} + v - \frac{uq}{p}. \tag{40}$$

From Eqs. (28) and (37), an analogous expression can be written relating $I^o_{\rm sym}$ and $K^o_{\rm sym}$, namely,

$$I^o_{\rm sym} = \frac{r}{p}K^o_{\rm sym} + s - \frac{rq}{p}. \tag{41}$$

Therefore, one sees for a fixed value of K_o that the bulk parameter $K^o_{\rm sym}$ is linearly correlated with $Q^o_{\rm sym}$ and $I^o_{\rm sym}$; see Fig. 11.

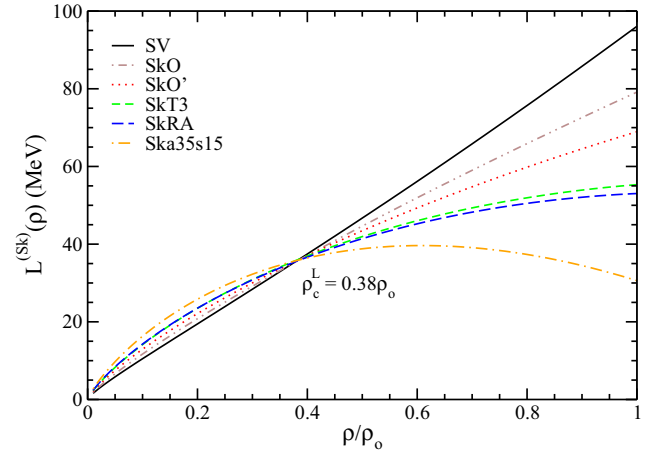

FIG. 6. (Color online) Symmetry energy slope as a function of ρ/ρ_o for some Skyrme parametrizations.

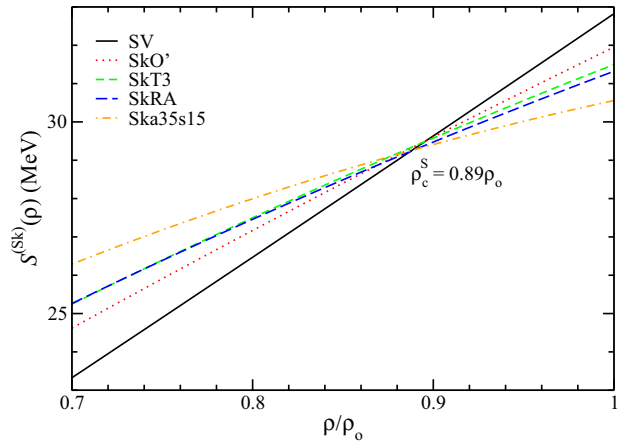

FIG. 8. (Color online) Symmetry energy as a function of ρ/ρ_o for some Skyrme parametrizations.

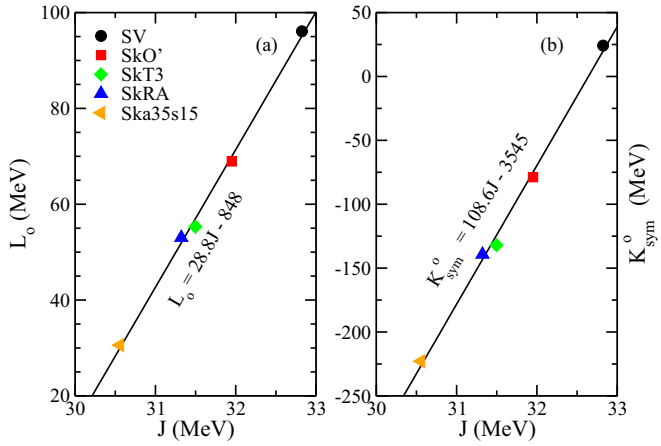

FIG. 9. (Color online) (a) L_o and (b) $K^o_{\rm sym}$ as a function of J for the Skyrme parametrizations of Fig. 8. The linear fits are indicated in each panel.

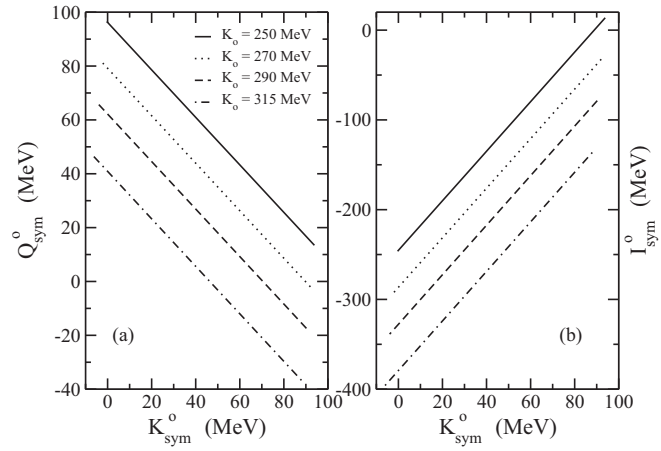

FIG. 11. (a) $Q^o_{\rm sym}$ and (b) $I^o_{\rm sym}$ as a function of $K^o_{\rm sym}$ for the NR limit. The effective mass varies in the range of $0.50 \leqslant m^* \leqslant 0.80$. For each panel, $\rho_o = 0.15$ fm^{-3} and $B_o = 16$ MeV.

Here we highlight that one can vary $K^o_{\rm sym}$ without any information regarding L_o. Let us remind the reader that $K^o_{\rm sym}$ can also be written only as a function of the isoscalar parameters, according to Eq. (12) of Ref. [12]. Thus, for fixed values of K_o, it is possible to investigate how $Q^o_{\rm sym}$ and $I^o_{\rm sym}$ depend on $K^o_{\rm sym}$ only from the variation of m^*.

Notice that, the expansion of $K^{\rm (NR)}_{\rm sym}/(3x+1)^2$ until order x^2 can describe the exact function in Eq. (24) in a density region of subsaturation densities; see Fig. 12(a). In spite of this, the quadratic equation constructed from the angular coefficients extracted from Fig. 11, namely, $1 - 0.88 x_c^{K_{\rm sym}} + \frac{2.76}{2!} x_c^{K_{\rm sym}{}^2} = 0$, presents no real roots, indicating no crossing points in the $K^{\rm (NR)}_{\rm sym}(\rho)$ function. This finding is confirmed in Fig. 12(b).

Another example of linear correlations between bulk parameters and the lack of crossing points in the density dependence in one of them, is the case of the quantities L_o and J. According to Eq. (26), a linear correlation between J and L_o is established if the function $b(m^*, \rho_o, B_o, K_o)$ is kept fixed, i.e., if the analyzed parametrizations have exactly the same isoscalar bulk parameters. Thus, parametrizations with different J values but the same isoscalar parameters present the behavior depicted in Fig. 13(a).

As one can see in Fig. 13(b), these parametrizations do not generate any crossing point in the density dependence of $\mathcal{S}(\rho)$. From the point of view of the discussion of Sec. II, one can understand the lack of crossing points from the equation $1 + 3x_c^{\rm S} = 0$, satisfied only for $x_c^{\rm S} = -\frac{1}{3}$, i.e., for $\rho_c^{\rm S}/\rho_0 = 0$ (because we have $\rho/\rho_0 = 3x + 1$).

In summary, one can associate linear correlations as signatures of crossing points only if the exact function studied can be approximated by its expansion and simultaneously if the equation $f(x_c) = 0$ presents nonzero real roots in the analyzed range of densities. In the case of the NR limit, the latter condition is not satisfied in the study of the $K^{\rm (NR)}_{\rm sym}(\rho)$ function, implying no crossing points in its density dependence in the range of subsaturation densities.

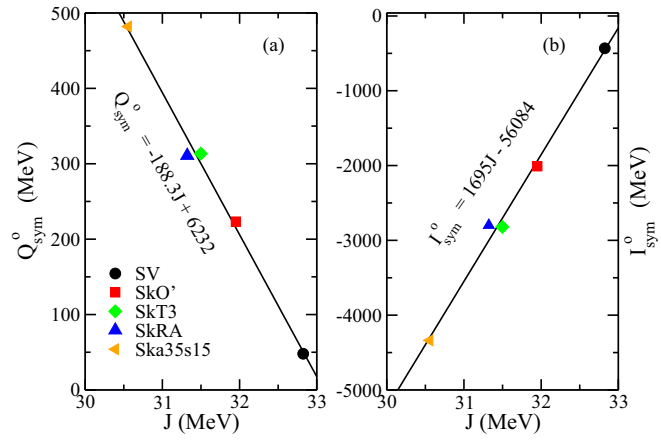

FIG. 10. (Color online) (a) $Q^o_{\rm sym}$ and (b) $I^o_{\rm sym}$ as a function of J for the Skyrme parametrizations of Fig. 8. The linear fits are indicated in each panel.

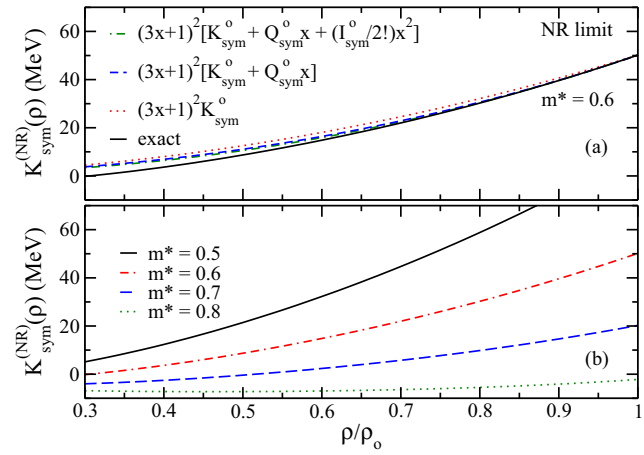

FIG. 12. (Color online) $K^{\rm (NR)}_{\rm sym}$ as a function of ρ/ρ_o. (a) Exact function for $m^* = 0.6$, Eq. (24), compared with its expansion. (b) Exact function for different effective mass values. The bulk parameters fixed in the two panels are $K_o = 270$ MeV, $\rho_o = 0.15$ fm^{-3}, and $B_o = 16$ MeV.

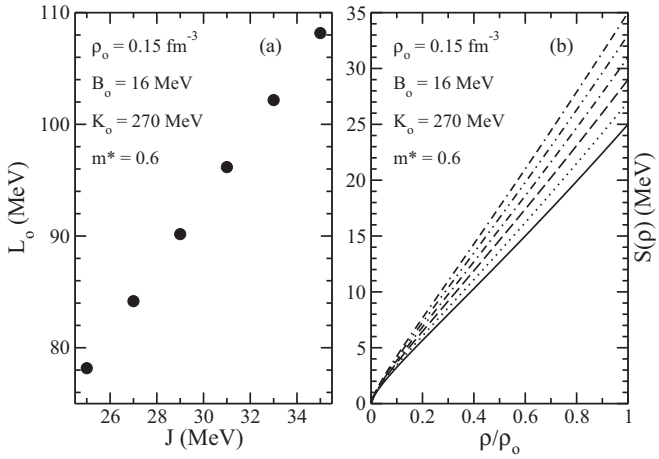

FIG. 13. (a) $L_o \times J$ correlation obtained from Eq. (26). (b) Density dependence of symmetry energy, Eq. (22).

C. Results from the isoscalar sector

Regarding the quantities related to the isoscalar sector of the nonrelativistic hadronic models, we underline here the relationship between K_o, Q_o, and I_o. For the former two quantities, a correlation was first found in Refs. [14,15] for some Skyrme parametrizations. In particular, they found it as a linear one. Here we proceed to find, in the NR limit framework, the conditions that the parametrizations must satisfy to give rise to the same relationship. For this purpose, we first need to obtain $Q(\rho,y)$ from the energy density, Eq. (18). This is done by calculating $Q = (3\rho)^3[\frac{\partial^3(\mathcal{E}/\rho)}{\partial\rho^3}]$ with the full expression given by

$$Q^{(\mathrm{NR})}(\rho,y) = -162B\rho^3 + \frac{12\lambda H_{5/3}}{5M^2}\rho^{\frac{2}{3}} \times\left(M - \frac{5}{4}G_S^2\rho + 20A\rho^2 + 165B\rho^3\right), \quad (42)$$

where Q_o is defined by $Q_o = Q^{(\mathrm{NR})}(\rho_o,1/2)$.

By using the coupling constants in terms of the bulk parameters in the expressions of K_o and Q_o, it is possible to find a relationship between these quantities,

$$Q_o = i(\rho_o)K_o + j(\rho_o,B_o,m^*), \quad (43)$$

where

$$i(\rho_o) = \frac{3\left(9M^2 - 73E_F^oM + 90E_F^{o2}\right)}{3M^2 - 19E_F^oM + 18E_F^{o2}}, \quad (44)$$

and

$$j(\rho_o,B_o,m^*) = \frac{1}{3M^2 - 19E_F^oM + 18E_F^{o2}} \times\left\{\frac{24E_F^o}{m^*}\left(M^2 - 40ME_F^o/3 + 60E_F^{o2}\right) - 162B_o\left(3M^2 - 25ME_F^o + 40E_F^{o2}\right) - 108E_F^o\left(M^2 - 10ME_F^o + 27E_F^{o2}\right)\right\}. \quad (45)$$

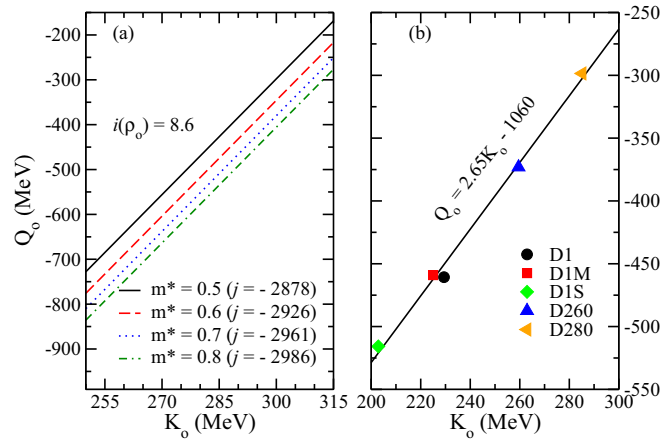

FIG. 14. (Color online) Q_o as a function of K_o for (a) the NR limit with different m^* values, and for (b) some Gogny parametrizations studied in Ref. [26]. In panel (a), $\rho_o = 0.15$ fm^{-3} and $B_o = 16$ MeV.

From the structure presented in Eq. (43), we notice that the effective mass plays a crucial role for the correlation between Q_o and K_o. For fixed values of m^*, this correlation is a linear one. We remember the reader that ρ_o and B_o vary only in a very narrow range around 0.15 fm^{-3} and 16 MeV, respectively. Thus, these bulk parameters can be considered constants for the hadronic mean-field models. For different m^* values, Eq. (43) generates parallel lines, as indicated in Fig. 14(a). The same linear correlation is also observed in some Gogny parametrizations, as indicated in Fig. 14(b).

From the perspective addressed in Sec. II, the linear correlation between K_o and Q_o could also be sought, by searching for a possible crossing point in the density dependence of the incompressibility. In fact, as pointed out in Fig. 15, there are two of them, at $\rho_c^{\mathrm{K}}/\rho_0 = 0.21$ (not shown), and $\rho_c^{\mathrm{K}}/\rho_0 = 0.79$. Furthermore, notice that the the second point is quite close to the crossing density $\rho_c^{\mathrm{K}}/\rho_0 = 0.71$ observed also for the Skyrme parametrizations studied in Ref. [14].

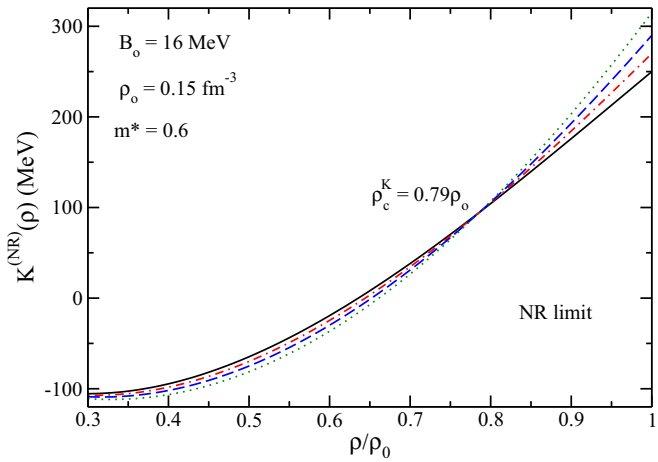

FIG. 15. (Color online) Incompressibility as a function of ρ/ρ_o for the NR limit, Eq. (21).

Because crossings in the $K^{(\mathrm{NR})}(\rho)$ function were found, they indicate a signature of a linear correlation, in this case at least between K_o and Q_o, because the latter is the bulk parameter associated with the immediately next order derivative of $K(\rho)$. Nevertheless, for the NR limit, we can also check analytically if the next bulk parameter, I_o, correlates with K_o. From Eq. (18) and the definition $I = (3\rho)^3[\frac{\partial^3(\mathcal{E}/\rho)}{\partial\rho^3}]$, one obtains

$$I^{(\mathrm{NR})}(\rho,y) = \frac{84\lambda H_{5/3}}{5M^2}\rho^{\frac{2}{3}}\left(-M + \frac{5}{7}G_{\mathrm{S}}^2\rho - \frac{20}{7}A\rho^2 + \frac{330}{7}B\rho^3\right). \quad (46)$$

From this expression, the fourth-order derivative of the energy per particle evaluated at the saturation density, $I_o = I^{(\mathrm{NR})}(\rho_o,1/2)$, can be written in terms of ρ_o, B_o, m^*, and K_o as

$$I_o = w(\rho_o)K_o + z(\rho_o,B_o,m^*), \quad (47)$$

where

$$w(\rho_o) = -\frac{20\left(25E_{\mathrm{F}}^oM - 54E_{\mathrm{F}}^{o2}\right)}{3M^2 - 19E_{\mathrm{F}}^oM + 18E_{\mathrm{F}}^{o2}}, \quad (48)$$

and

$$z(\rho_o,B_o,m^*) = \frac{1}{3M^2 - 19E_{\mathrm{F}}^oM + 18E_{\mathrm{F}}^{o2}} \times\left\{\frac{40E_{\mathrm{F}}^o}{m^*}\left(3M^2 - 56ME_{\mathrm{F}}^o + 324E_{\mathrm{F}}^{o2}\right) + 1080B_o\left(9ME_{\mathrm{F}}^o - 32E_{\mathrm{F}}^{o2}\right) - 72E_{\mathrm{F}}^o\left(4M^2 - 77ME_{\mathrm{F}}^o + 324E_{\mathrm{F}}^{o2}\right)\right\}. \quad (49)$$

Notice that, once more, the effective mass needs to be constant for the parametrizations to ensure a linear dependence between I_o and K_o, with the angular coefficient given by $w(0.15) = -4.16$.

For the sake of completeness, we use the angular coefficients $i(\rho_o)$ and $w(\rho_o)$ to calculate the crossing density in Fig. 15. First, we consider the energy per particle of symmetric nuclear matter as

$$E(\rho) \simeq E_o + \frac{K_o}{2!}x^2 + \frac{Q_o}{3!}x^3 + \frac{I_o}{4!}x^4; \quad (50)$$

then the corresponding expansion for $K(\rho)$ reads

$$K(\rho) = 18\rho\frac{\partial E}{\partial\rho} + 9\rho^2\frac{\partial^2E}{\partial\rho^2} = 6(3x+1)\frac{\partial E}{\partial x} + (3x+1)^2\frac{\partial^2E}{\partial x^2} \quad (51)$$

$$\simeq (3x+1)\left[K_o + (9K_o + Q_o)x + \left(6Q_o + \frac{I_o}{2}\right)x^2 + \frac{5I_o}{2}x^3\right]. \quad (52)$$

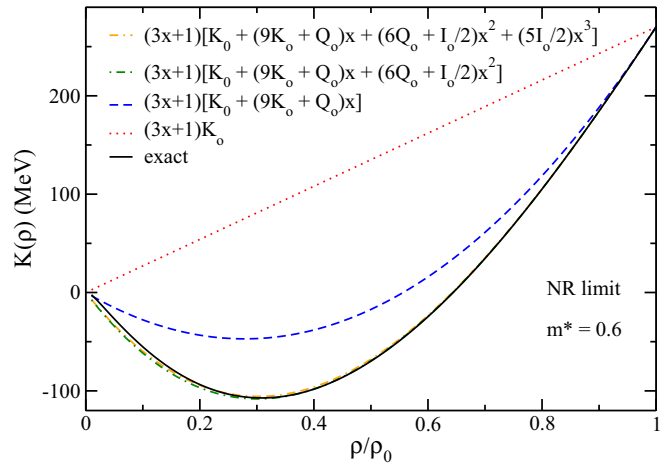

FIG. 16. (Color online) Density dependence of the incompressibility compared with its expansion for the NR limit.

This expansion is observed to be consistent with the exact function, Eq. (21), as shown in Fig. 16.

It is worth noting that despite the extra term in Eq. (51) compared with $\mathcal{F}''$ in Eq. (5), the final expansion, Eq. (52), is analogous to the general function $\mathcal{F}^{(m)}(\rho)$ in Eq. (7). Therefore, all the procedure developed in Sec. II also applies in the analysis of correlations and crossing points for the $K^{(\mathrm{NR})}(\rho)$ function in the isoscalar sector. Indeed, this was done for some Skyrme parametrizations in Ref. [14]. From this point of view, it is possible to use Eqs. (43) and (47) to rewrite Eq. (52) as

$$K(\rho) = (3x+1) \times\left\{K_o\left[1 + (9+i)x + \left(6i + \frac{w}{2}\right)x^2 + \frac{5w}{2}x^3\right] + \left[j + \left(6j + \frac{z}{2}\right)x + \frac{5z}{2}x^2\right]x\right\}. \quad (53)$$

Thus, the crossings points in Fig. 15(a) are justified if $1 + (9+i)x_c^{\mathrm{K}} + (6i + w/2)x_c^{\mathrm{K}2} + (5w/2)x_c^{\mathrm{K}3} = 0$. Two solutions of this cubic equation are $\rho_c^{\mathrm{K}}/\rho_0 = 0.21$ and $\rho_c^{\mathrm{K}}/\rho_0 = 0.79$.

IV. CORRELATIONS IN FR-RMF MODELS

In the context of quantum hadrodynamics (QHD), protons and neutrons are the fundamental particles interacting each other through scalar and vector meson exchange. In this framework, the fields σ and ω represent, respectively, these mesons and mimic the attractive and repulsive parts of the nuclear interaction. The main representative of QHD models is the Walecka one [5], in which the only two free parameters are fitted to reproduce the values of ρ_o and B_o. However, it does not give reasonable values for K_o ($\sim$500 MeV) and M_o^* ($\sim 0.54M$). This problem was circumvented by Boguta and Bodmer [13], who added to the Walecka model cubic and quartic self-interactions in the scalar field σ, introducing, consequently, two more free parameters, which are fitted so as to fix these quantities. All thermodynamic quantities of this

model are found from its Lagrangian density, given by

$$\mathcal{L} = \overline{\psi}(i\gamma^\mu\partial_\mu - M)\psi + g_\sigma\sigma\overline{\psi}\psi + \frac{1}{2}\left(\partial^\mu\sigma\,\partial_\mu\sigma - m_\sigma^2\sigma^2\right) - \frac{A}{3}\sigma^3 - \frac{B}{4}\sigma^4 - g_\omega\overline{\psi}\gamma^\mu\omega_\mu\psi - \frac{1}{4}F^{\mu\nu}F_{\mu\nu} + \frac{1}{2}m_\omega^2\omega_\mu\omega^\mu - \frac{g_\rho}{2}\overline{\psi}\gamma^\mu\vec{\rho}_\mu\vec{\tau}\psi - \frac{1}{4}\vec{B}^{\mu\nu}\vec{B}_{\mu\nu} + \frac{1}{2}m_\rho^2\vec{\rho}_\mu\vec{\rho}^\mu, \quad (54)$$

with $F_{\mu\nu} = \partial_\nu\omega_\mu - \partial_\mu\omega_\nu$ and $\vec{B}_{\mu\nu} = \partial_\nu\vec{\rho}_\mu - \partial_\mu\vec{\rho}_\nu - g_\rho(\vec{\rho}_\mu \times \vec{\rho}_\nu)$. The coupling constants are g_σ, g_ω, g_ρ, A, and B. For a complete description of the model, and also other kinds of FR-RMF ones, such as density dependent, crossed terms, and NLPCs, we address the reader to the recent study of Ref. [6] involving an analysis of 263 relativistic parametrizations under constraints related to symmetric nuclear matter, pure neutron matter, symmetry energy, and its derivatives. Here we mainly focus on searching for correlations between bulk parameters for the FR-RMF parametrizations described by Eq. (54).

A. Isovector sector

Besides its complete analytical structure, another advantage of the NR limit of NLPC models is its usefulness in predictions of correlations in Boguta-Bodmer models, as pointed out in Ref. [12]. For instance, the $L_o \times J$ correlation in Eq. (26) is shown to be linear also for these models under the restriction of fixed values of effective mass. Like in the NR limit, different values for K_o do not destruct the linear dependence; see Fig. 2(b) of Ref. [12]. Based on this correspondence, we use the framework of the NR limit to confirm other correlations in Boguta-Bodmer models. Still at the isovector sector, we showed in Ref. [12] that the linear correlation indicated in Eq. (28) holds for the models described by Eq. (54) if we also fix the values of K_o and J. Now we further investigate such a correlation. In Fig. 17, we show $K^o_{\rm sym}$ as a function of L_o for parametrizations with effective masses submitted to the FRS constraint, Eq. (1). According to Ref. [10], this is the range of m^* in which Boguta-Bodmer models have to be constrained to produce spin-orbit splittings in agreement with well-established experimental values for the ^{16}O, ^{40}Ca, and ^{208}Pb nuclei. In this figure, we present curves corresponding to the limiting values of the ranges $25 \leqslant J \leqslant 35$ MeV [6] and $250 \leqslant K_o \leqslant 315$ MeV [29].

From these results, we can conclude that the relation $K^o_{\rm sym} = p_{\rm rel}L_o + q_{\rm rel}$ also works well for the Boguta-Bodmer models submitted to the FRS constraint. However, by comparing the angular coefficients $p(\rho_o)$ from Eq. (28) and $p_{\rm rel}$, we notice that $p_{\rm rel}$ slightly depends on K_o, unlike the nonrelativistic case in which the angular coefficient depends only on ρ_o. We perform the same analysis for the L_o dependence on $Q^o_{\rm sym}$, motivated by the linear correlation presented in Eq. (31). The result is found in Fig. 18. As we see, there is a correlation between $Q^o_{\rm sym}$ and L_o. However, the linear form $Q^o_{\rm sym} = u_{\rm rel}L_o + v_{\rm rel}$ is strongly dependent on K_o, unlike the previous case. For $K_o = 315$ MeV, for example,

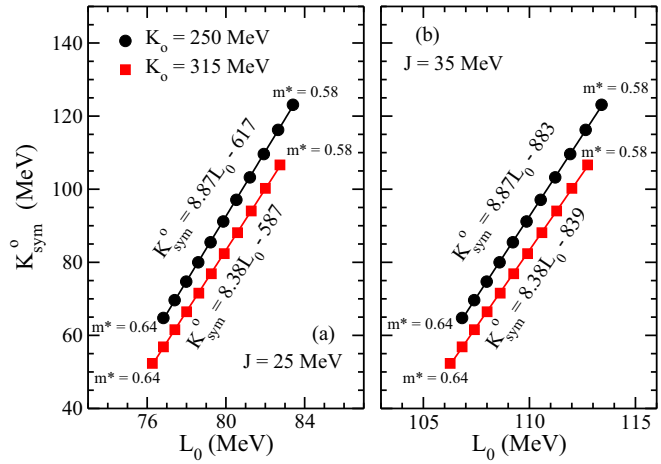

FIG. 17. (Color online) $K^o_{\rm sym}$ versus L_o for Boguta-Bodmer models with $\rho_o = 0.15$ fm^{-3} and $B_o = 16$ MeV. The linear fittings are indicated in both panels.

we notice the range of effective mass that still ensures that a line in the curve fitting is reduced from the range of Eq. (1) to $0.60 \leqslant m^* \leqslant 0.64$. The break of this linearity is better depicted in the insets of Fig. 18.

One can also use the linear dependencies shown in Figs. 17 and 18, with the latter guaranteed only for some values of K_o and m^*, to justify a possible crossing point in the density dependence of the symmetry energy slope, as we did in the case of nonrelativistic models in Sec. III. In fact, there is such a crossing, as we can see in Fig. 19. From the angular coefficients of the respective lines of Figs. 17(a) and 18(a), we can solve the equation $1 + 8.87x_c^{\rm L} + \frac{16.86}{2!}x_c^{\rm L\,2} = 0$ to find a crossing density at $\rho_c^{\rm L}/\rho_0 = 0.61$. This value cannot be refined because a linear correlation is not found in the next order bulk parameter, namely, $I^o_{\rm sym}$, as we see in Fig. 20. We see that

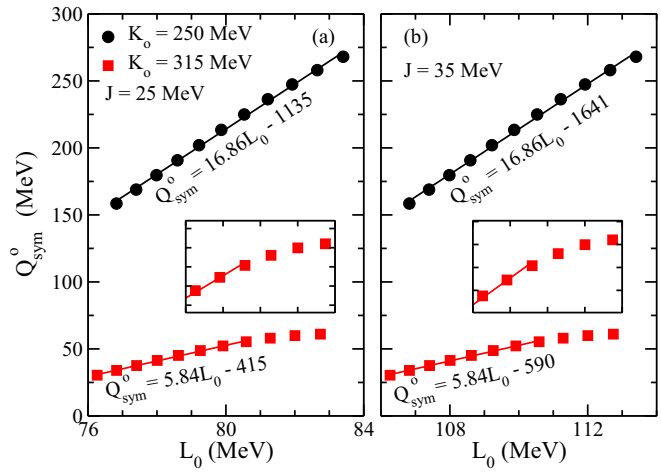

FIG. 18. (Color online) $Q^o_{\rm sym}$ versus L_o for Boguta-Bodmer models with $\rho_o = 0.15$ fm^{-3}, $B_o = 16$ MeV, and $0.58 \leqslant m^* \leqslant 0.64$. The linear fittings are indicated in both panels. In the insets, we show L_o in the ranges of (a) $79 \leqslant L_o \leqslant 83$ MeV and (b) $109 \leqslant L_o \leqslant 113$ MeV.

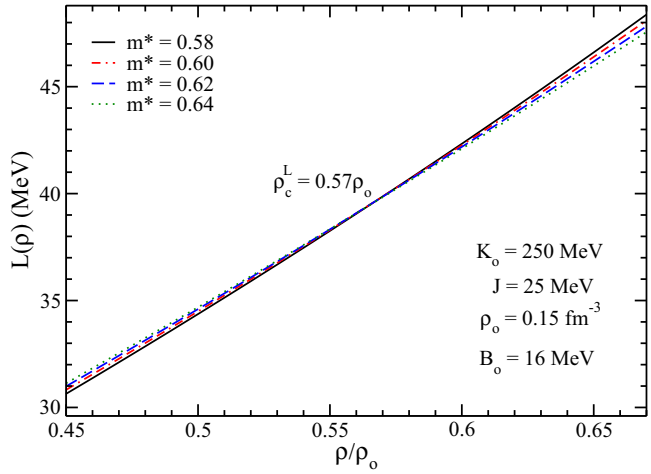

FIG. 19. (Color online) Symmetry energy slope as a function of ρ/ρ_o for some Boguta-Bodmer parametrizations.

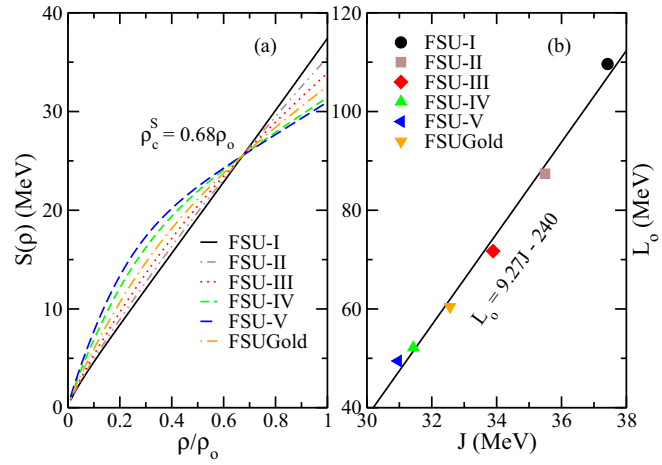

FIG. 21. (Color online) (a) Symmetry energy as a function of ρ/ρ_o and (b) L_o as a function of J for the parametrizations of Ref. [35].

a correlation between L_o and $I_{\rm sym}^o$ holds for the relativistic Boguta-Bodmer models, but it is not a linear one, as we verified in the NR limit, Eq. (37).

Still concerning isovector bulk parameters, we point out to the reader a specific class of relativistic models of Ref. [35] with mesonic crossed interactions. Following the notation of Ref. [6], they are classified as type 4 models ($\sigma^3+\sigma^4+\omega_0^4+$ cross terms models) and have the terms

$$\mathcal{L}_{\sigma\omega\rho} = g_\sigma g_\omega^2 \sigma\omega_\mu\omega^\mu\left(\alpha_1+\frac{1}{2}\alpha_1' g_\sigma\sigma\right) + \frac{C}{4}\left(g_\omega^2\omega_\mu\omega^\mu\right)^2 + \frac{1}{2}\alpha_3' g_\omega^2 g_\rho^2\omega_\mu\omega^\mu\vec{\rho}_\mu\vec{\rho}^\mu + g_\sigma g_\rho^2\sigma\vec{\rho}_\mu\vec{\rho}^\mu\left(\alpha_2+\frac{1}{2}\alpha_2' g_\sigma\sigma\right) \quad (55)$$

added to the Lagrangian density of Eq. (54). The parametrizations of this model presented in Ref. [35] are constructed to fix the symmetry energy not at the saturation density, but in a smaller value. They present $\mathcal{S}(\rho_c^S) = 26$ MeV, with $\rho_c^S/\rho_o = 0.68$. Therefore, the $\mathcal{S}(\rho)$ function presents a crossing point, as pointed out in Ref. [16], and as one can see in Fig. 21(a). Therefore, such a crossing indicates a linear behavior between L_o and J for these specific parametrizations. This correlation is clearly observed in Fig. 21(b). Furthermore, the crossing density is obtained from the angular coefficient, by solving the equation $1+9.27x_c^S = 0$. The solution of this linear equation leads to $\rho_c^S/\rho_0 = 0.68$, exactly the value verified in Fig. 21(a).

As a last remark of this section, we point out to the reader that the angular and linear coefficients of the $L_o \times J$ correlation are not universal, as we can see by comparing the linear equation of Fig. 21(b) of the relativistic FSU family, with that of Fig. 9(a) of the Skyrme parametrizations. Even among relativistic models, one cannot reach such universality, as we can see by the comparison of the correlation in Fig. 21(b) with that found in Ref. [36] for the relativistic NL3* and IU-FSU families.

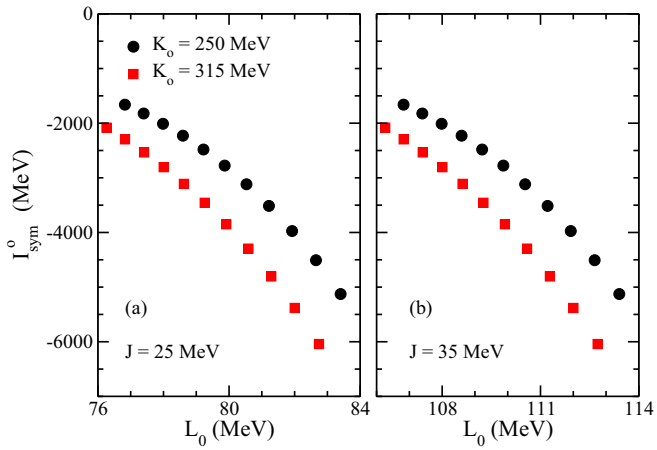

FIG. 20. (Color online) $I_{\rm sym}^o$ versus L_o for Boguta-Bodmer models with $\rho_o = 0.15$ fm^{-3}, $B_o = 16$ MeV, and $0.58 \leqslant m^* \leqslant 0.64$.

B. Isoscalar sector

Motivated by the analytical structure relating K_o, Q_o, and I_o, we investigate in this section whether the linear dependencies presented in the NR limit [see Eqs. (43) and (47)] also applies for Boguta-Bodmer models. According to the NR limit case, if we keep fixed the effective mass, K_o linearly correlates with Q_o, as we show in Eq. (43) and Fig. 14(a). For the relativistic case of FR-RMF models described by Eq. (54), we see that this condition remains, as one can see in Fig. 22(a) for the MS2 [37], NLSH [38], NL4 [39], NLRA1 [40], Q1 [41], Hybrid [42], NL3 [38], FAMA1 [43], NL-VT1 [44], NL06 [6], and NLS [45] parametrizations presenting $m^* \simeq 0.6$. Such a correlation can be used to justify the crossing in the $K(\rho)$ function depicted in Fig. 22(b). Proceeding in that direction, we use the expansion of the energy per particle in Eq. (50) until order x^3 to calculate the density dependence of the incompressibility. The result of this calculation is given by

$$K(\rho) \simeq (3x+1)[K_o + (9K_o + Q_o)x + 6Q_o x^2]. \quad (56)$$

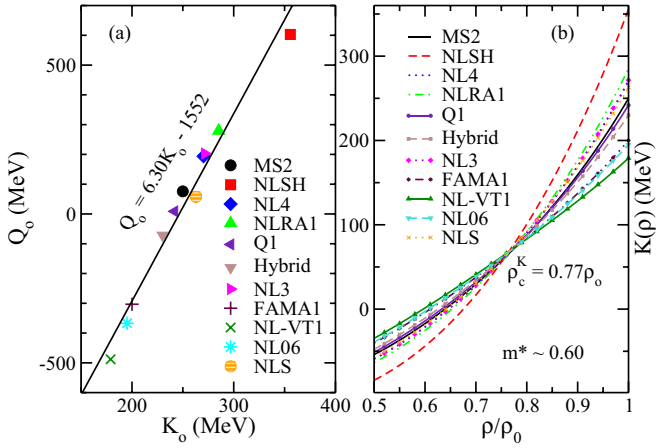

FIG. 22. (Color online) (a) Q_o as a function of K_o for some Boguta-Bodmer parametrizations with $m^* \simeq 0.6$. (b) Incompressibility as a function of ρ/ρ_o for the same parametrizations.

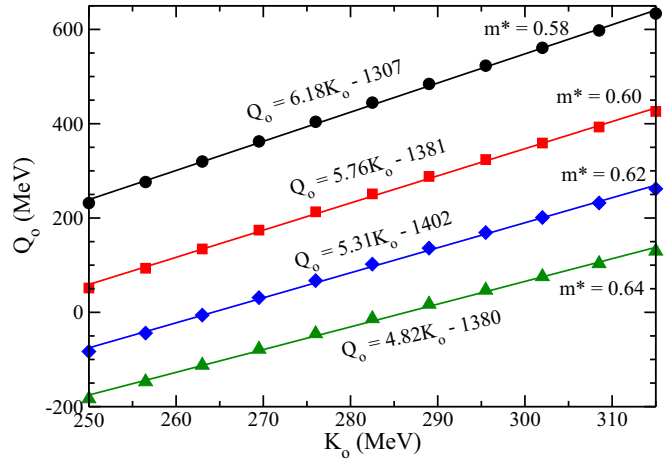

FIG. 23. (Color online) Q_o as a function of K_o for Boguta-Bodmer parametrizations in which $\rho_o = 0.15$ fm^{-3} and $B_o = 16$ MeV. The linear fittings are indicated in the figure.

Therefore, the linear dependence $Q_o = i_{\rm rel}K_o + j_{\rm rel}$ shown in Fig. 22(a) can be used in Eq. (56) to furnish

$$K(\rho) \simeq (3x+1)\{K_o[1+(9+i_{\rm rel})x+6ix^2] + (1+6x)j_{\rm rel}x\}, \quad (57)$$

with $i_{\rm rel} = 6.30$ and $j_{\rm rel} = 1552$ MeV. Thus, one has a crossing point when the quadratic equation $1+(9+i_{\rm rel})x_c^{\rm K} + 6i_{\rm rel}x_c^{\rm K2} = 0$ present solution. This is the case for $\rho_c^{\rm K}/\rho_0 = 0.78$.

We remark that a crossing point in the $K(\rho)$ function was first explained from the linear correlation between K_o and Q_o in Ref. [14]. However, the authors found such a crossing for some nonrelativistic Skyrme and Gogny parametrizations. For the relativistic models analyzed, they did not find linear correlations or crossing points. Indeed, for the nonrelativistic case, they found a crossing at $\rho_c^{\rm K}/\rho_0 \simeq 0.7$, a value quite close to our findings, namely, $\rho_c^{\rm K}/\rho_0 = 0.77$ and $\rho_c^{\rm K}/\rho_0 = 0.79$, for Boguta-Bodmer models and the NR limit, respectively; see Figs. 22(b) and 15.

Unlike the linear correlation presented in the NR limit, the angular coefficient $i_{\rm rel}$ is slightly dependent on the effective mass. For the former case, we have $i = i(\rho_o)$; see Eq. (44). In Fig. 23, we show this variation observing the FRS constraint and the range $250 \leqslant K_o \leqslant 315$ MeV. In particular, notice that for $m^* = 0.64$, a value that ensures good values for finite nuclei spin-orbit splittings [10], the range of the skewness coefficient is given by $-183 \leqslant Q_o \leqslant 130$ MeV. Such a specific constraint for Q_o presents an overlap of $\simeq$36% with a recent range proposed for this bulk parameter in Ref. [46], namely, $-494 \leqslant Q_o \leqslant -10$ MeV. In this study, the authors analyzed models with crossed interactions among the fields, i.e., models described by Eq. (54) added to the terms in Eq. (55). They verified that such models, presenting the skewness coefficient in the range of $-494 \leqslant Q_o \leqslant -10$ MeV, satisfy the suprasaturation constraint for the density dependence of the pressure in the symmetric nuclear [47] and the neutron star mass constraints, given by $2.01 \pm 0.04 M_\odot$. This latter is attributable to the recently discovered neutron star PSR J0348 + 0432 [48].

Finally, we verify whether the relationship between K_o and I_o presented in Eq. (47) is preserved in the relativistic case. According to the results of Fig. 24(a), we see that the linear behavior $I_o = w_{\rm rel}K_o + z_{\rm rel}$ still remains in the range of $250 \leqslant K_o \leqslant 315$ MeV, with $w_{\rm rel}$ slightly depending on m^*, like in the case of $i_{\rm rel}$.

It is worth noticing that, as shown in Fig. 24(b), for a broader range of K_o the linear dependence is blurred, although a correlation between the bulk parameters K_o and I_o still remains.

V. MODELS WITH MORE THAN ONE ISOVECTOR COUPLING CONSTANT

In previous sections, we have analyzed under what conditions the linear correlations presented in the NR limit

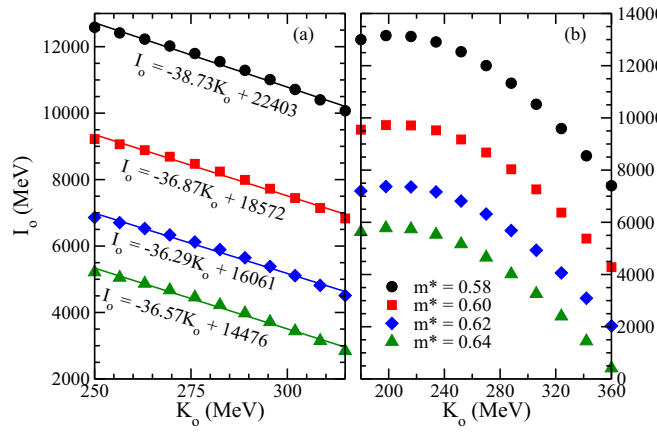

FIG. 24. (Color online) I_o as a function of K_o for Boguta-Bodmer parametrizations in which $\rho_o = 0.15$ fm^{-3} and $B_o = 16$ MeV. The curves are constructed in the range of (a) $250 \leqslant K_o \leqslant 315$ MeV and (b) $180 \leqslant K_o \leqslant 360$ MeV. The linear fittings are indicated in panel (a).

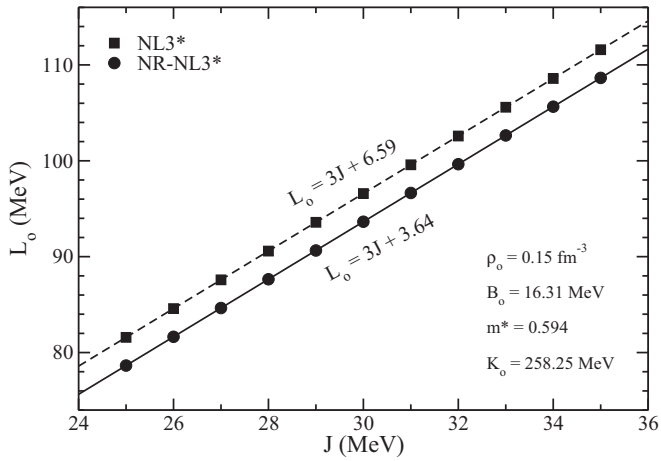

FIG. 25. L_o as a function of J for the NL3* Boguta-Bodmer parametrizations and their NR limit versions NR-NL3*. These parametrizations were constructed by fixing $\rho_o = 0.15$ fm^{-3}, $B_o = 16.31$ MeV, $m^* = 0.594$, and $K_o = 258.25$ MeV and by running J.

of point-coupling models are reproduced in the context of relativistic Boguta-Bodmer parametrizations. However, our comparisons were restricted to relativistic and nonrelativistic models presenting only one isovector coupling constant, namely, g_ρ and $G_{\rm TV}^2$, respectively. For the Boguta-Bodmer model, g_ρ is related to the interaction strength between the nucleon and the ρ meson. For the NR limit model, $G_{\rm TV}^2$ regulates the strength of the term that mimics the same kind of interaction (we remind the reader that our NR limit model is derived from a relativistic point-coupling model, therefore, a model in which there are no meson exchanges). Regarding the specific relationship between L_o and J, we concluded in Ref. [12] that for the NR limit model, such correlation is linear whenever the isoscalar bulk parameters, namely, m^*, ρ_o, B_o, and K_o, remain unchanged. We also showed that this same condition also ensures a linear correlation between L_o and J for Boguta-Bodmer parametrizations. Furthermore, the angular coefficients of these correlations are the same, and the absolute values of L_o are very close to each other, as we can see in Fig. 25 for the NL3* Boguta-Bodmer parametrizations and their respective NR limit versions, namely, the NR-NL3* ones.

To construct this figure, we fixed the isoscalar parameters values of the NL3* model and varied the J values. We used such a procedure for the exact relativistic NL3* parametrization and for its NR limit version. For the latter, we used our Eq. (26).

By proceeding one step further in our analysis of the $L_o \times J$ correlation, we now study relativistic and nonrelativistic models with more than one isovector parameter to verify whether the dependence observed in Fig. 25 still applies. For the relativistic model, we use that described by the Lagrangian density of Eq. (54) added to those of Eq. (55) with $\alpha_1 = \alpha_2 = \alpha_1' = \alpha_2' = C = 0$; i.e., we choose a model with interaction between the mesons ω and ρ. Thus, we are dealing with a model with two isovector parameters, namely, g_ρ and α_3'.

To take the NR limit of this specific model, we construct a point-coupling Lagrangian density,

$$\begin{aligned}\mathcal{L}_{\rm NLPC} = {}& \bar\psi(i\gamma^\mu\partial_\mu - M)\psi - \frac{1}{2}G_{\rm V}^2(\bar\psi\gamma^\mu\psi)^2 + \frac{1}{2}G_{\rm S}^2(\bar\psi\psi)^2 \\ & + \frac{A}{3}(\bar\psi\psi)^3 + \frac{B}{4}(\bar\psi\psi)^4 - \frac{1}{2}G_{\rm TV}^2(\bar\psi\gamma^\mu\vec\tau\psi)^2 \\ & - \frac{1}{4}G_{\rm VTV}(\bar\psi\gamma^\mu\vec\tau\psi)^2(\bar\psi\gamma^\mu\psi)^2, \end{aligned} \tag{58}$$

in which the last term mimics the interaction between the mesons ω and ρ. The isovector coupling constants of this model are $G_{\rm TV}^2$ and $G_{\rm VTV}$. The symmetry energy and its slope for the NR limit of this model are given by

$$\mathcal{S}^{(\rm NR)}(\rho) = G_{\rm TV}^2\rho + G_{\rm VTV}\rho^3 + \frac{\lambda\rho^{\frac{2}{3}}}{6M^*(\rho,1/2)} \tag{59}$$

and

$$\begin{aligned} L^{(\rm NR)}(\rho) = {}& \frac{\lambda\rho^{\frac{2}{3}}}{3M^2}\left(M + \frac{5}{2}G_{\rm S}^2\rho + 8A\rho^2 + \frac{33}{2}B\rho^3\right) \\ & + 3G_{\rm TV}^2\rho + 9G_{\rm VTV}\rho^3, \end{aligned} \tag{60}$$

respectively. The new isovector coupling constant, $G_{\rm VTV}$, is found by imposing upon the model that the symmetry energy at $\rho_1/\rho_o \equiv r$ is fixed at a particular value $\mathcal{S}_1 \equiv \mathcal{S}(\rho_1)$. Here r is a value smaller than 1. Furthermore, we still found $G_{\rm TV}^2$ by requiring that the model present a particular value J for the symmetry energy at the saturation density. The analytical form of these constants as a function of the bulk parameters can be found in the Appendix.

Such an analytical structure enables us to find a correlation between L_o and J,

$$L_o = 3\left(\frac{3-r^2}{1-r^2}\right)J + b'(m^*,\rho_o,B_o,K_o,r,\mathcal{S}_1), \tag{61}$$

with

$$\begin{aligned} & b'(m^*,\rho_o,B_o,K_o,r,\mathcal{S}_1) \\ & = b(m^*,\rho_o,B_o,K_o) + \frac{10E_{\rm F}^o r^{2/3}}{3(r^2-1)\left(3M^2 - 19E_{\rm F}^oM + 18E_F^{o2}\right)} \\ & \times\left\{\frac{E_{\rm F}^o}{3m^*}\left(13M - 66E_{\rm F}^o\right) + \frac{K_o}{6}\left(M - 6E_{\rm F}^o\right)\right. \\ & - B_o\left(9M - 48E_{\rm F}^o\right) - E_{\rm F}^o\left(7M - 36E_{\rm F}^o\right) \\ & - r\left[\frac{16E_{\rm F}^o}{3m^*}\left(M - 6E_{\rm F}^o\right) + \frac{2}{3}K_o\left(M - 3E_{\rm F}^o\right)\right. \\ & \left. - 6B_o\left(3M - 13E_{\rm F}^o\right) - 2E_{\rm F}^o\left(5M - 27E_{\rm F}^o\right)\right] \\ & - r^2\left[-\frac{E_{\rm F}^o}{m^*}\left(M - 10E_{\rm F}^o\right) - \frac{K_o}{2}\left(M - 2E_{\rm F}^o\right)\right. \\ & \left.\left. + 3B_o\left(3M - 10E_{\rm F}^o\right) + 3E_{\rm F}^o\left(M - 6E_{\rm F}^o\right)\right]\right\} + \frac{6}{(r^2-1)} \\ & \times\left[\frac{\mathcal{S}_1}{r} + \frac{5E_{\rm F}^o}{9m^*}(1 - r^{2/3}) + \frac{5E_{\rm F}^o}{9}(r^{2/3} - r^{-1/3})\right]. \end{aligned} \tag{62}$$

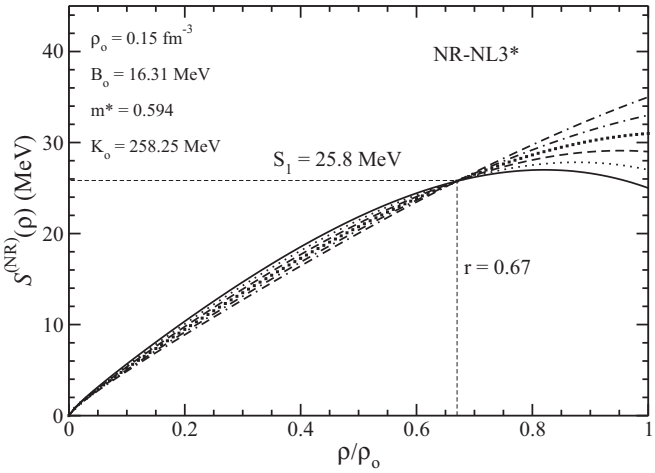

FIG. 26. Density dependence of the symmetry energy for the NR-NL3* parametrization family with two isovector parameters.

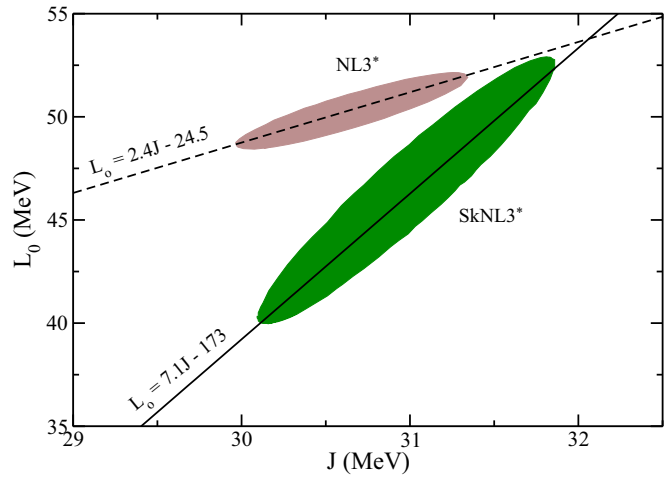

FIG. 28. (Color online) Correlation bands for the L_o and J bulk parameters of the NL3* parametrization family and SkNL3* one, extracted from Fig. 3(a) of Ref. [36]. The solid lines are linear fits.

Notice that now a linear correlation between L_o and J is established if the function $b'(m^*, \rho_o, B_o, K_o, r, \mathcal{S}_1)$ is a constant, i.e., if the quantities m^*, ρ_o, B_o, K_o, r, and $\mathcal{S}_1$ are kept fixed. Moreover, if we now look at the $\mathcal{S}(\rho)$ function for a particular parametrization family, namely, that in which the set m^*, ρ_o, B_o, K_o, r, and $\mathcal{S}_1$ is fixed and J runs a certain range, we see a crossing point, differently from the NR limit case presenting only one isovector coupling constant. We show this finding in Fig. 26 for the NR-NL3* family.

By looking at the FR relativistic model with the ω and ρ mesons interaction, we verified that a linear correlation between L_o and J also holds if we apply the same conditions observed in the NR limit case, i.e., fixed values of m^*, ρ_o, B_o, K_o, r, and $\mathcal{S}_1$. A direct comparison between these two correlations, analogous to that presented in Fig. 25, is displayed in Fig. 27. Here we restricted our analysis for J in a range of values greater than $\mathcal{S}_1$.

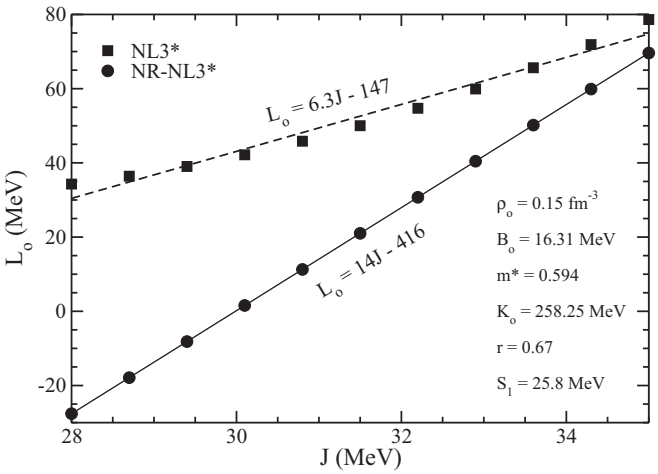

FIG. 27. L_o as a function of J for the relativistic NL3* parametrization family and their NR limit versions NR-NL3*. These parametrizations were constructed by fixing $\rho_o = 0.15$ fm^{-3}, $B_o = 16.31$ MeV, $m^* = 0.594$, $K_o = 258.25$ MeV, $r = 0.67$, $\mathcal{S}_1 = 25.8$ MeV, and by running J. Both models present two isovector coupling constants.

From Fig. 27, we can notice that the NR limit version of NL3* parametrizations with two isovector coupling constants presents a different slope for the $L_o \times J$ linear correlation, differently from the case shown in Fig. 25, where we tested models with only one isovector parameter. This result is in qualitative agreement with the findings obtained in Ref. [36], where the authors compared the same NL3* parametrization family (two isovector parameters) with a nonrelativistic Skyrme parametrization family named as SkNL3*. For this family, the isoscalar bulk parameters present the same values as in the relativistic NL3* model. The authors also imposed that the energy per neutron predictions, at subsaturation densities, of the SkNL3* and NL3* models were compatible with the band constraint depicted in Fig. 2 of Ref. [36]. As a consequence, they found correlation bands (ellipses) for the L_o and J bulk parameters, as one can see in Fig. 28.

These ellipses were constructed by the authors of Ref. [36] from the covariance analysis method. In Fig. 28, we extracted such bands and constructed the linear fits. Notice the nonrelativistic line presenting a greater slope in comparison with the relativistic one, exactly the same qualitative behavior observed in Fig. 27, where we have constructed the correlations only observing the conditions under which they are linear ones. Furthermore, our ratio for the NL3* slope to the NR-NL3* one is not much different to the same ratio of Fig. 28, namely, 2.22 for ours (Fig. 27) and 2.96 for Ref. [36], or Fig. 28, obtained from the covariance analysis method.

VI. SUMMARY AND CONCLUSIONS

In this work, we analysed the arising of correlations between isovector and isoscalar bulk parameters of hadronic nonrelativistic and relativistic mean-field models. In particular, we discussed the connection of the crossing point in the

density dependence of a particular bulk quantity, with the specific linear correlation between this quantity with its immediately next order bulk parameter. In the isovector sector, for instance, if there is a crossing point in the density dependence of the symmetry energy, then it can be explained by the linear correlation between the symmetry energy, $\mathcal{S}$, and its slope, $L = 3\rho(\partial\mathcal{S}/\partial\rho)$, both evaluated at the saturation density; i.e., there will be a linear correlation between $J = \mathcal{S}(\rho_o)$ and $L_o = L(\rho_o)$. In summary, the crossing points can be seen as a signature, or a route, in the searching of linear correlations among bulk parameters, as discussed in Sec. II.

In the nonrelativistic framework, we presented correlations in some Skyrme [3] and Gogny parametrizations [see Figs. 2, 7, 9, 10, and 14(b)], as well as in parametrizations generated from the NR limit of NLPC models. By using the analytical structure of the latter model, we could write its five coupling constants in terms of the bulk parameters ρ_o, B_o, K_o, m^*, and J to investigate the conditions under which the linear correlations of L_o with $K^o_{\rm sym}$, $Q^o_{\rm sym}$, and $I^o_{\rm sym}$, in the isovector sector, and of K_o with Q_o and I_o, in the isoscalar one, hold. For these parametrizations, we showed that L_o linearly correlates with $K^o_{\rm sym}$, $Q^o_{\rm sym}$, and $I^o_{\rm sym}$ if we keep fixed the values of J and K_o; see Eqs. (28), (31), and (37). Following analogous procedure, we found that parametrizations with fixed effective mass lead to linear correlations of K_o with Q_o and I_o, according to Eqs. (43) and (47), and the respective subsequent discussions. For some of these linear correlations, we discussed how they could have been found from the searching of crossing points in the bulk parameter as a function of the density. We pointed out that the crossing at $\rho_c^{\rm L}/\rho_0 = 0.47$ ($\rho_c^{\rm K}/\rho_0 = 0.79$) exhibited in Fig. 3 (Fig. 15) for the $L^{(\rm NR)}$ ($K^{(\rm NR)}$) function, for instance, is a signature of the linear correlations between L_o and $K^o_{\rm sym}$ (K_o and Q_o), at least.

Regarding the RMF models [6], we mainly studied that presenting cubic and quartic self-interaction in the scalar field σ, namely, the Boguta-Bodmer model [13]. The reason for this choice was based on our previous work of Ref. [12]. In that work, we showed that some correlations among bulk parameters presented in the NR limit of NLPC models are also valid for this particular relativistic model. We further studied the correlations for bulk parameters of isovector and isoscalar sectors, mainly in the ranges of effective mass, symmetry energy, and incompressibility given by $0.58 \leqslant m^* \leqslant 0.64$, $25 \leqslant J \leqslant 35$ MeV, and $250 \leqslant K_o \leqslant 315$ MeV, respectively. The first range was proved to be experimentally consistent with finite nuclei spin-orbit splittings, according to Ref. [10]. The second is compatible with experimental values from analyses of different terrestrial nuclear experiments and astrophysical observations [6,28], and the latter was based on the recent reanalysis of data on isoscalar giant monopole resonance energies [29].

In the isovector sector, we showed that L_o also correlates with $K^o_{\rm sym}$, $Q^o_{\rm sym}$, and $I^o_{\rm sym}$ like in the NR limit. However, the linear behavior of L_o with $I^o_{\rm sym}$ is broken in the range of m^* and K_o analyzed, as pointed out in Fig. 20. For the correlation between L_o and $Q^o_{\rm sym}$, we verified that the linear behavior is blurred only at higher values of K_o; see Fig. 18. We still concluded that the linear dependence of L_o on $K^o_{\rm sym}$ is preserved for fixed values of J, as in the case of the NR limit, according to the results presented in Fig. 17. This specific linear correlation was used to justify the crossing point exhibited in Fig. 19 for the $L(\rho)$ function.

By comparing the behavior of K_o and Q_o in the isoscalar sector, we verified that these quantities are linearly correlated if the effective mass is kept fixed, exactly as deduced in the NR limit case. This correlation was displayed in Figs. 22(a) and 23. We also used the angular coefficient presented in the former figure to justify the crossing point in the incompressibility function of the parametrizations shown in Fig. 22(b). Furthermore, we notice that for $m^* = 0.64$ and $250 \leqslant K_o \leqslant 315$ MeV, Q_o varies in the range of $-183 \leqslant Q_o \leqslant 130$ MeV, and present an overlap of about 36% with the range of $-494 \leqslant Q_o \leqslant -10$ MeV recently proposed in Ref. [46].

Last, we verified that the linear behavior between K_o and I_o is still valid for the Boguta-Bodmer models with fixed effective mass and for the range of $250 \leqslant K_o \leqslant 315$ MeV; see Fig. 24(a). Nevertheless, the linearity is broken for a broader range of K_o but with a correlation $I_o = I_o(K_o)$ still applying; see Fig. 24(b).

ACKNOWLEDGMENTS

We thank the support from Coordenação de Aperfeiçoamento de Pessoal de Nível Superior (CAPES) and Conselho Nacional de Desenvolvimento Científico e Tecnológico (CNPq) of Brazil. O.L. also acknowledges the support of Grant No. 2013/26258-4 from São Paulo Research Foundation (FAPESP). M.D. acknowledges support from Fundação de Amparo à Pesquisa do Estado do Rio de Janeiro (FAPERJ), Grant No. 111.659/2014.

APPENDIX: COUPLING CONSTANTS OF THE NR LIMIT

In the NR limit of the NLPC models, the coupling constants can be written in terms of the bulk parameter, namely, m^*, ρ_o, B_o, K_o, and J, as

$$G^2_{\rm TV} = \frac{J}{\rho_o} - \frac{\lambda}{6M}\frac{1}{m^*}\rho_o^{-\frac{1}{3}}, \tag{A1}$$

$$A = \frac{M/3\rho_o^2}{\left(3M^2 - 19E^o_{\rm F}M + 18E^{o2}_{\rm F}\right)}\left\{\frac{8E^o_{\rm F}}{m^*}\left(M - 6E^o_{\rm F}\right) + K_o\left(M - 3E^o_{\rm F}\right) - 9B_o\left(3M - 13E^o_{\rm F}\right) - 3E^o_{\rm F}\left(5M - 27E^o_{\rm F}\right)\right\}, \tag{A2}$$

$$B = \frac{M/3\rho_o^3}{\left(3M^2 - 19E^o_{\rm F}M + 18E^{o2}_{\rm F}\right)}\left\{-\frac{E^o_{\rm F}}{m^*}\left(M - 10E^o_{\rm F}\right) - \frac{K_o}{2}\left(M - 2E^o_{\rm F}\right) + 3B_o\left(3M - 10E^o_{\rm F}\right) + 3E^o_{\rm F}\left(M - 6E^o_{\rm F}\right)\right\}, \tag{A3}$$

$$G_{\rm S}^2 = \frac{M}{\rho_o}\left(\frac{1}{m^*} - 1\right) - 2A\rho_o - 3B\rho_o^2, \tag{A4}$$

and

$$G_{\rm V}^2 = \frac{M}{\rho_o}\left(\frac{1}{m^*} - 1\right) - \frac{E_{\rm F}^o}{m^*\rho_o} - \frac{B_o}{\rho_o} - A\rho_o - 2B\rho_o^2. \tag{A5}$$

In the case of the NR limit obtained from the Lagrangian density of Eq. (58), the two isovector coupling constants are written as

$$G_{\rm VTV} = \left\{J - \frac{\mathcal{S}_1}{r} - \frac{5E_{\rm F}^o}{9m^*}(1-r^{2/3}) - \frac{5E_{\rm F}^o}{9M}\left[M\left(1-\frac{1}{r}\right) + 2A\rho_o^2(1-r) + 3B\rho_o^3(1-r^2)\right]r^{2/3}\right\}\frac{1}{\rho_o^3(1-r^2)}, \tag{A6}$$

and

$$G_{\rm TV}^2 = \frac{J}{\rho_o} - \frac{\lambda}{6M}\frac{1}{m^*}\rho_o^{-\frac{1}{3}} - G_{\rm VTV}\rho_o^2, \tag{A7}$$

with $r = \rho_1/\rho_o$ and $\mathcal{S}_1 = \mathcal{S}(\rho_1)$.

[1] P. Ring and P. Schuck, *The Nuclear Many-Body Problem* (Springer, Heidelberg, 1980).
[2] M. Naghdi, Phys. Part. Nucl. **45**, 924 (2014).
[3] M. Dutra, O. Lourenço, J. S. Sá Martins, A. Delfino, J. R. Stone, and P. D. Stevenson, Phys. Rev. C **85**, 035201 (2012).
[4] J. Dechargé and D. Gogny, Phys. Rev. C **21**, 1568 (1980).
[5] J. D. Walecka, Ann. Phys. **83**, 491 (1974).
[6] M. Dutra, O. Lourenço, S. S. Avancini, B. V. Carlson, A. Delfino, D. P. Menezes, C. Providência, S. Typel, and J. R. Stone, Phys. Rev. C **90**, 055203 (2014).
[7] J. A. Tjon, Phys. Lett. B **56**, 217 (1975); R. Perne and H. Kroger, Phys. Rev. C **20**, 340 (1979); J. A. Tjon, Nucl. Phys. A **353**, 47 (1981).
[8] A. Delfino, T. Frederico, V. S. Timóteo, and L. Tomio, Phys. Lett. B **634**, 185 (2006).
[9] F. Coester, S. Cohen, B. D. Day, and C. M. Vincent, Phys. Rev. C **1**, 769 (1970).
[10] R. J. Furnstahl, J. J. Rusnak, and B. D. Serot, Nucl. Phys. A **632**, 607 (1998).
[11] C. J. Horowitz and J. Piekarewicz, Phys. Rev. Lett. **86**, 5647 (2001).
[12] B. M. Santos, M. Dutra, O. Lourenço, and A. Delfino, Phys. Rev. C **90**, 035203 (2014).
[13] J. Boguta and A. R. Bodmer, Nucl. Phys. A **292**, 413 (1977).
[14] E. Khan and J. Margueron, Phys. Rev. C **88**, 034319 (2013).
[15] E. Khan, J. Margueron, and I. Vidaña, Phys. Rev. Lett. **109**, 092501 (2012).
[16] J. Piekarewicz, Phys. Rev. C **83**, 034319 (2011).
[17] B. A. Brown, Phys. Rev. Lett. **85**, 5296 (2000).
[18] E. Khan, M. Grasso, and J. Margueron, Phys. Rev. C **80**, 044328 (2009).
[19] J. J. Rusnak and R. J. Furnstahl, Nucl. Phys. A **627**, 495 (1997).
[20] D. G. Madland, T. J. Bürvenich, J. A. Maruhn, and P.-G. Reinhard, Nucl. Phys. A **741**, 52 (2004).
[21] O. Lourenço, M. Dutra, A. Delfino, and R. L. P. G. Amaral, Int. J. Mod. Phys. E **16**, 3037 (2007).
[22] P. W. Zhao, Z. P. Li, J. M. Yao, and J. Meng, Phys. Rev. C **82**, 054319 (2010).
[23] T. Niksic, D. Vretenar, and P. Ring, Prog. Part. Nucl. Phys. **66**, 519 (2011).
[24] B. A. Nikolaus, T. Hoch, and D. G. Madland, Phys. Rev. C **46**, 1757 (1992).
[25] B. K. Agrawal, S. Shlomo, and V. K. Au, Phys. Rev. C **72**, 014310 (2005); L. W. Chen and J. Z. Gu, J. Phys. G **39**, 035104 (2012).
[26] R. Sellahewa and A. Rios, Phys. Rev. C **90**, 054327 (2014).
[27] Zhen Zhang and Lie-Wen Chen, Phys. Rev. C **90**, 064317 (2014).
[28] B.-A. Li and X. Han, Phys. Lett. B **727**, 276 (2013).
[29] J. R. Stone, N. J. Stone, and S. A. Moszkowski, Phys. Rev. C **89**, 044316 (2014).
[30] C. Ducoin, J. Margueron, C. Providência, and I. Vidaña, Phys. Rev. C **83**, 045810 (2011).
[31] M. Beiner, H. Flocard, N. Van Giai, and P. Quentin, Nucl. Phys. A **238**, 29 (1975).
[32] P.-G. Reinhard, D. J. Dean, W. Nazarewicz, J. Dobaczewski, J. A. Maruhn, and M. R. Strayer, Phys. Rev. C **60**, 014316 (1999).
[33] F. Tondeur, M. Brack, M. Farine, and J. M. Pearson, Nucl. Phys. A **420**, 297 (1984).
[34] M. Rashdan, Mod. Phys. Lett. A **15**, 1287 (2000).
[35] B.-J. Cai and L.-W. Chen, Phys. Rev. C **85**, 024302 (2012).
[36] F. J. Fattoyev, W. G. Newton, J. Xu, and B. A. Li, Phys. Rev. C **86**, 025804 (2012).
[37] H. Müller and B. D. Serot, Nucl. Phys. A **606**, 508 (1996).
[38] G. A. Lalazissis, J. König, and P. Ring, Phys. Rev. C **55**, 540 (1997).
[39] B. Nerlo-Pomoroska and J. Sykut, Int. J. Mod. Phys. E **13**, 75 (2004).
[40] M. Rashdan, Phys. Rev. C **63**, 044303 (2001).
[41] R. J. Furnstahl, B. D. Serot, and H. B. Tang, Nucl. Phys. A **615**, 441 (1997).
[42] J. Piekarewicz and M. Centelles, Phys. Rev. C **79**, 054311 (2009).
[43] J. Piekarewicz, Phys. Rev. C **66**, 034305 (2002).
[44] M. Bender, K. Rutz, P. G. Reinhard, J. A. Maruhn, and W. Greiner, Phys. Rev. C **60**, 034304 (1999).
[45] P.-G. Reinhard, Z. Phys. A **329**, 257 (1988).
[46] B. J. Cai and L. W. Chen, arXiv:1402.4242v1.
[47] P. Danielewicz, R. Lacey, and W. G. Lynch, Science **298**, 1592 (2002).
[48] J. Antoniadis *et al.*, Science **340**, 6131 (2013).